약학박사 학위논문

Kinetics of the Absorption, Distribution, Metabolism and Excretion of Lobeglitazone, a Novel Activator of Peroxisome Proliferator-activated Receptor Gamma in Rats

PPAR(peroxisome proliferator-activated receptor)-γ 활성제 Lobeglitazone 의 흡수, 분포, 대사 및 배설의 체내동태 연구

2015 년 2 월

서울대학교 대학원

제약학과 약제과학 전공

이 종 화

ABSTRACT

Kinetics of the Absorption, Distribution, Metabolism and Excretion of Lobeglitazone, a Novel Activator of Peroxisome Proliferator-activated Receptor Gamma in Rats

Jong-Hwa Lee

Department of Pharmaceutical Sciences

College of Pharmacy

The Graduate School

Seoul National University

This primary goal of this study was to determine the biopharmaceutical properties of lobeglitazone (LB) in rats. LB is a novel thiazolidinedione (TZD)-based activator of the peroxisome proliferator-activated receptor gamma (PPAR-γ) that interacted multidrug resistance protein (MDR1) and organic anion transporting polypeptide (OATP1B1) transporters in a parallel artificial membrane permeability assay (PAMPA) and Madin-Darby canine kidney (MDCK) cells permeability assays. The present findings demonstrate that LB had an IC_{50} value of approximately 12.5 ± 3.61 μM in MDR1

expressing MDCK cells, adequate stability in rat liver microsomes (56% remaining at 30 min), and appeared to be metabolized by cytochrome P450 (CYP). A CYP inhibitory potency experiment indicated that LB was primarily interacted with CYP1A2, CYP2C9 and CYP2C19. In addition, LB had an absolute bioavailability of approximately 95% after oral administration, which indicates that it was readily absorbed, and exhibited linear pharmacokinetics following the intravenous (IV) administration of 0.5-2 mg/kg. Rat plasma samples were processed using a fast flow protein precipitation (FF-PPT) method and then introduced onto an LC-MS/MS system for quantification using the validated assay. The primary distribution site for LB was the liver, but it was also distributed to the heart, lungs, and fat tissue. The excretion values of LB to the urine, bile, feces, and intestine were relatively insignificant (< 10% of the dose).

The present findings suggest that, although LB interacts with several drug transporters and metabolizing enzymes, its pharmacokinetics were linear with a high oral bioavailability. The formation of the metabolites of LB by demethylation and hydroxylation after incubation of LB within rat liver microsomes was elucidated. The plasma concentrations of LB after oral administration of 0.1-10 mg/kg were markedly higher (3.9-5.4 fold) in female rats. An *in vitro* metabolic stability study found that the CL_{int} value for females was approximately 29% of the value for males. Similarly, the

apparent oral clearance for females was approximately 20% of that for males. These observations suggested that there are clear gender differences in the pharmacokinetics and hepatic metabolism for LB in rats.

These kinetics of the absorption, distribution, metabolism and excretion of LB demonstrated the characterization of LB to develop as an oral diabetes agent.

Keywords: Lobeglitazone (LB), Pharmacokinetics, ADME, Gender differences, LC-MS/MS, Transporters, CYP enzymes, P-glycoprotein, Microsomal stability

Student Number: 2007-30464

CONTENTS

List of Tables

List of Figures

Abbreviations

ADME	absorption, distribution, metabolism and excretion
BCRP	breast cancer resistance protein
CO_2	carbon dioxide
CYP	cytochrome P450
DMEM	Dulbecco’s modified eagle’s medium
DMSO	dimethyl sulfoxide
HBSS	Hank’s balanced salts solution
HEPES	N-2-hydroxyethylpiperazine-N'-2-ethane sulfonic acid
HPLC	high performance liquid chromatography
IC_{50}	concentration resulting in 50% inhibition
LB	lobeglitazone
LC-MS/MS	liquid chromatography-tandem mass spectrometry
logP	partition coefficient
LOQ	limit of quantification
MDCK	Madin-Darby canine kidney

MDR	multidrug resistance protein
MRM	multiple reaction monitoring
NADPH	nicotinamide adenine dinucleotide phosphate-oxidase
OAT	organic anion transporter
OATP	organic anion transporting polypeptide
OCT	organic cation transporter
PAMPA	parallel artificial membrane permeability assay
P-gp	P-glycoprotein
RED	rapid equilibrium dialysis
TEER	transepithelial electrical resistance
TZD-PPAR	thiazolidinedione-peroxisome proliferator-activated receptors
UGT	UDP-glucuronosyltransferase
WT	wild type

1. INTRODUCTION

1.1. Lobeglitazone

Diabetes is characterized by failure of the pancreas to produce insulin (type 1) or enough adequately functioning insulin (type 2) to enable glucose and fats from food to enter the cells of the body for energy. As a result, glucose and lipid levels remain high.

Type 1 diabetes occurs when the body's immune system kills the pancreatic cells that produce insulin. Subsequently, blood glucose must be regulated by treatment with insulin treatment in combination with a balanced diet and physical activity. If glucose levels become too low, the resulting hypoglycaemia can lead to unconsciousness, but if the glucose levels become too high, the resulting hyperglycaemia will cause the body to break down fat reserves for use as energy instead of glucose. This, in turn, leads to release of toxic ketones and acids (ketoacidosis), which can result in coma and death. At present, the prevention type 1 diabetes is not possible, and these patients must be treated with insulin the rest of their lives.

Type 2 diabetes is much more common, and accounts for 95-98% of all patients with diabetes. In type 2 diabetes, blood glucose levels begin to rise as the pancreas weakens due to aging or the added demands introduced by a

lack of exercise and increasing amounts of abdominal fat. Abdominal fat releases free fatty acids and hormones into the circulatory system, which in turn, reduces the effectiveness of insulin, enhancing the release of glucose from the liver, and stimulating other destabilizing effects. In addition, once blood glucose levels rise, the circulating glucose itself attacks the pancreas and cause further damage to the insulin-producing beta cells. Recent studies on the progression of type 2 diabetes have shown that insulin resistance in peripheral tissues induces compensatory hyperinsulinemia, which instigates the failure of β-islet cells and leads to prandial pain and obvious fasting hyperglycemia (Harris et al., 1998; Jay and Ren, 2007).

The currently available oral drugs for type 2 diabetes that are recommended by the American Diabetes Association (Association, 2010) include six classes of drugs that lower blood glucose levels via various mechanisms: sulfonylureas, biguanides, metaglitanides, α-glucosidase inhibitors, dipeptidyl peptidase (DPP)-4 inhibitors, and thiazolidinediones. Of these drugs, TZD derivatives such as troglitazone (Rezulin®), pioglitazone (Actos®), and rosiglitazone (Avandia®) operate via a novel mechanism that improves insulin resistance, in a notably different manner than existing medication. Peroxisome proliferator-activated receptors (PPARs), which are largely expressed in adipose tissue than in skeletal muscle and liver tissue, are ligand-inducible transcription factors that belong to the nuclear hormone

receptor superfamily (Hevener et al., 2007; Norgren et al., 1994). It appears that TZD-based PPAR activators intensify the action of insulin and promote the utilization of glucose in peripheral tissues (Ferre, 2004; Orasanu et al., 2008). As a result, these types of drugs may be useful for the management of type 2 diabetes.

Lobeglitazone (LB), an activator of TZD-peroxisome proliferator-activated receptor-gamma (TZD-PPAR-γ), is a new drug in development for the treatment of diabetes in Korea. LB has 1.11-fold and 16.6-fold higher affinities for PPAR-γ than pioglitazone and rosiglitazone, respectively, which are the current TZD-PPARs activators in clinical use. Thus, provided that the kinetic properties of LB are comparable to other PPAR activators, it is expected that LB would have a lower effective dose and fewer cardiovascular side effects (viz, common for TZD-PPARs activators), which are common for TZD-PPAR activators, than other TZD analogues (Kim et al., 2004; Kim et al., 2003; Lee et al., 2007; Lee et al., 2005; Sauerberg et al., 2003). Unfortunately, comprehensive pharmacokinetic studies of TZD-PPAR activators, including LB, have yet to be conducted.

The metabolic characteristics and biopharmaceutical properties of TZD-PPARs activators are relatively well understood. For example, while pioglitazone and rosiglitazone are primarily eliminated via hepatic metabolism, the major cytochrome P450 (CYP) isozymes involved in the

elimination of these factors are different; CYP2C8/3A4 is associated with pioglitazone action and CYP2C8/2C9 is associated with rosiglitazone action. Although pioglitazone and rosiglitazone possess a common TZD moiety, they have different side chains that appear to be the main determinant of heterogeneity in their various metabolic outcomes. TZD-PPARs activators are relatively hydrophobic; the logP values for rosiglitazone, pioglitazone and troglitazone determined using ALOGPS 2.1 software are 2.95, 3.17 and 4.16, respectively. In addition, the degrees of absorption were 95%, 83%, and 50% for rosiglitazone, pioglitazone, and troglitazone, respectively (Cox et al., 2000; Hanefeld, 2001; Loi et al., 1999), which are relatively high values. However, the involvement of transporters in the pharmacokinetics of TZD-PPARs activators has yet to be systemically studied.

1.2. Absorption, Distribution, Metabolism and Excretion

The absorption, distribution, metabolism and excretion (ADME) properties of a drug are important factors during the conventional drug discovery process, and insufficiencies in this properties are the primary reason behind the high attrition rate of drugs under development, which is approximately 90% (DiMasi, 2001). The cost of failure at this stage is enormous, and the inefficiencies involved in the drug development process represent a major

contributing factor to the high research and development budgets of pharmaceutical companies.

A crucial component of the ADME properties of a drug is its passage across cell membranes. Therefore, it is essential to consider the mechanisms by which drugs cross membranes, and the physicochemical properties of molecules and membranes that influence this transport. The important characteristics of a drug include its molecular size and shape, solubility at the site of absorption, degree of ionization, and the relative lipid solubilities of its ionized and non-ionized forms. When a drug permeates a cell, it must transverse the cellular plasma membrane as well as other barriers that can include a single layer of cells (intestinal epithelium) or several layers of cells (skin). Despite various structural differences, the diffusion and transport of different drugs across these boundaries share many common characteristics, including two major mechanisms: passive transport and active transport. The passive transport of a drug is induced by differences in electrochemical potentials, whereas the active transport of a drug involves membrane transporters.

The systemic absorption of a drug is dependent upon its physicochemical properties such as the nature of the drug product, the anatomical environment, and the physiological functions at the site of drug absorption (Benet, 1978). During the drug discovery process, the typical route of drug administration is

oral. LB has been developed for oral administration; thus, the measurement of its absolute oral bioavailability is important in this process. After a drug is absorbed or injected into the bloodstream, it is distributed into various tissues or organs via systemic circulation, and different patterns of drug distribution reflect the particular physiological factors and physicochemical properties of a drug. Following its absorption and distribution, a drug is eliminated from the body via metabolism and excretion.

Drug metabolism plays a central role in modern drug discovery and candidate optimization. In fact, recent reviews have detailed how metabolism has impacted the discovery and design process and the challenges that the field will face in the future (Baillie, 2006; Caldwell et al., 2009; Sun and Scott, 2010; Tang and Lu, 2009; Zhang et al., 2009). It is also important for the design of regulatory toxicology and first-in-human studies because they can influence factors such as choice of species, dose selection, and which metabolites are important to monitor in early studies (Baillie, 2009; Walker et al., 2009; Zhu et al., 2009).

Drug metabolism tends to transform xenobiotics into products that are more polar and water-soluble so that the metabolites are easily and readily excreted (Commandeur et al., 1995; Lennard, 1993; Park et al., 2001). Phase I reactions introduce or expose functional groups such as hydroxyl, amino, carbonyl, or sulfhydryl groups via hydrolysis, oxidation, and reduction

reactions, whereas phase II reactions are conjugation reactions. Many metabolites that are the result of phase I processing are not sufficiently hydrophilic to be eliminated via urine or bile, and thus, phase II reactions usually involve the addition of a large polar group. Here, a conjugation reaction with an endogenous substrate, such as glucuronic acid, sulfuric acid, or an amino acid, results in polarity and the creation of water-soluble compounds that are typically therapeutically inactive. Transferase enzymes such as uridine diphosphoglucuronosyl transferases (UGTs), N-acetyl transferases (NATs), glutathione S-transferases (GSTs), and sulfotransferases are responsible for the majority of phase II reactions. Cytochrome P450 enzymes account for approximately 75% of total metabolism making them the major enzymes involved in drug metabolism (Williams et al., 2004). A majority of drugs undergo deactivation by CYPs, either directly or by facilitated excretion from the body, whereas conversely, many types of substances are bioactivated by CYPs to form their active compounds (Furge and Guengerich, 2006; Guengerich, 2008).

Drugs are eliminated from the body in either an unchanged form or as various metabolites. Excretory organs, except for the lungs, eliminate polar compounds more efficiently than substances with high lipid solubility, and thus, lipid-soluble drugs are not readily eliminated until they are metabolized into more polar compounds. Renal excretion and biliary excretion are two

major elimination routes, whereas routes such as sweat, saliva, and tears are quantitatively unimportant.

1.3. Metabolite Identification

It has been estimated that for every 5000 new chemical entities evaluated in a discovery program, only one is approved for the market. Even after a drug is released, it is possible that the drug could be withdrawn from the market or acquire a warning label (black box) due to adverse drug reactions that were not previously observed. Recent examples of drugs withdrawn from the market due to hepatotoxicity include troglitazone, nefazodone, and pemoline (Wysowski and Swartz, 2005). Thus, in the pharmaceutical industry, the understanding that drug metabolites often play critical roles in the efficacy and side effects of drugs has made drug metabolism research an integral part of modern drug research.

A number of *in vitro* and *in vivo* biotransformation techniques are available for the generation of metabolites. The *in vitro* techniques utilize subcellular fractions prepared from cells that mediate drug metabolism, intact cell-based systems, intact organs, and isolated expressed enzymes, whereas the *in vivo* methods involve the use of biological fluids (e.g., plasma, bile, urine) obtained from laboratory animals or humans dosed with the parent molecule. Recently, techniques using liquid chromatography linked with

tandem mass spectrometry (LC-MS/MS) have begun to play a dominant role in the detection, identification, and quantification of metabolites. Due to the sensitivity and selectivity of LC-MS/MS, this technique allows for the detection of low concentrations of an analyte using short chromatographic run times. Furthermore, the sample preparation tends to be less difficult, because most biologically active compounds are readily ionized during the LC-MS/MS process. In addition to being convenient, the LC-MS/MS sample preparation procedures are generic which makes them ideal for both targeted screening and general unknown drug screening.

Targeted screening is a directed screening approach that analyzes samples for specific drugs. This approach is often referred to as multi-target screening, and currently constitutes the majority of screening tests performed. When performed on an LC-MS/MS system, targeted screening methods typically employ the multiple reaction monitoring (MRM) mode of operation, which provides superior sensitivity and selectivity, and enables the detection of low concentrations of drugs in complex biological matrices. However, because this approach only detects a priori selected compounds, it will not reveal the presence of a compound not included in the target drug list.

General unknown screening does not rely upon a target compound list, and as a result, this type of analysis is sensitive to the detection of unexpected pharmaceuticals, nutritional supplement-based analytes, and designer drugs.

When performed on an LC-MS/MS system, unknown screening methods typically employ full-scan MS experiments to detect all of the major components present in a sample, including unexpected compounds. The downside to this approach is a slight compromise in the level of detection that is primarily due to a reduction in selectivity that is inherent when performing single-MS, rather than MS/MS experiments. For many applications, this is a minor limitation given the benefit of identifying unanticipated analytes.

1.4. Gender Differences

Sex-related differences in drug metabolism have been known for more than 60 years, but it was not until recently that the mechanisms for these differences were explored (Shapiro et al., 1995; Skett, 1988). Recent studies have shown that sexual dimorphism in rats, and possibly in other species, results from the differential expression of sex-dependent hepatic cytochrome P450s. This differential expression, in turn, is largely influenced by steroid and pituitary hormone levels and profiles. Evidence has shown that the sexual dimorphic secretion pattern of growth hormone directly regulates the expression of certain hepatic cytochrome P450s (Legraverend et al., 1992; Waxman, 1992).

The pharmacokinetics of TZD-PPAR activators, such as rosiglitazone and pioglitazone, have observed gender differences in both humans and rats

(Fujita et al., 2003; Patel et al., 1999; Vlckova et al., 2010). In humans, the kinetic differences were associated with pharmacodynamic differences as evidenced by the fact that rosiglitazone and pioglitazone were more effective for females than in males (Patel et al., 1999; Vlckova et al., 2010). Although the underlying reasons for these gender differences have yet to be fully elucidated, there are a number of possible mechanisms including differences in body fat distribution (Adams et al., 1997; MacKellar et al., 2009; Mori et al., 1999) and sex hormones (Anderson et al., 2001; Benz et al., 2012; Soldin et al., 2011). In addition, the pharmacokinetic differences could be mediated by gender-specific variation in hepatic metabolism, which is the primary pathway for the elimination of drugs (Baldwin et al., 1999; Baughman et al., 2005; Cox et al., 2000; Kim et al., 2011).

1.5. Objectives of the Study

The primary objective of the present study was to characterize the biopharmaceutical properties of LB. In addition to being important for a full understanding of the pharmacokinetics of a drug, these types of properties may also be closely linked to clinically relevant issues such as drug-drug interactions in the later stages of new drug development. The *in vitro* properties of the metabolism including metabolite identification and transport of LB, and their relationship to its pharmacokinetics were of particular

interest in the present study because this information may directly influence the elucidation, and/or prediction of drug interactions. In addition, the present study also investigated whether there were gender differences in the *in vitro* hepatic metabolism and pharmacokinetics of LB.

2. MATERIALS AND METHODS

2.1. Chemicals and Reagents

LB (98.5% purity), LB sulfate (99.1% purity) and rosiglitazone [99.0% purity, an internal standard (IS) of LB assay] were provided by Chong Kun Dang Pharmaceuticals (Seoul, Korea). Dulbecco's modified Eagle's medium (DMEM), N-2-hydroxyethylpiperazine-N'-2-ethanesulfonic acid (HEPES), testosterone and 7-hydroxy coumarin, were purchased from Sigma-Aldrich (St. Louis, MO, USA). Pooled male and female rat liver microsomes, and uridine diphosphate (UDP) reaction mix solution were purchased from Corning Gentest (Woburn, MA, USA). Blank rat plasma samples containing heparin were obtained from the Korea Institute of Toxicology (Daejeon, Korea). Solvents were of HPLC grade (Fisher Scientific, Pittsburgh, PA, USA), and other chemicals were of the highest grade available.

2.2. Quantification of LB in Rat Plasma Using a Liquid-Chromatography/Tandem Mass Spectrometry

2.2.1. Liquid Chromatography Conditions

An HPLC system (HP1100; Agilent Technologies, Santa Clara, CA, USA), consisting of a binary pump, an online degasser, an auto-sampler, and a column heater, equipped a reversed phase HPLC column (Zorbax C18, 2.1

mm×100 mm, 3.5 μm; Agilent Technologies) for the chromatographic separation of LB and the IS was used in the study. The mobile phase was composed of acetonitrile-water-formic acid (60:40:0.25, v/v/v) and eluted at a flow rate of 0.2 mL/min. In this study, the sample volume was set at 5 μL, and the analytical column and samples were maintained at 30°C and 20°C, respectively.

2.2.2. Mass Spectrometer Conditions

Mass spectrometric detection was performed with a quadrupole mass spectrometer (Quattro Micro; Waters, Milford, MA, USA), equipped with an electro-spray ionization (ESI) source operating in the positive-ion mode. In this study, the spectrometer was set in the MRM mode. The settings of the mass spectrometer for LB were 3.5 kV for the capillary voltage, 40 V for the cone voltage, 200 ms for the dwell time, 40 V for the collision energy, 120°C for the source temperature and 300°C for the desolvation temperature. The analytical conditions for the IS were identical to those for LB, except for the collision energy of 30 V. In this study, MRM *m/z* transitions at 482→258 for LB and 358→135 for the IS were simultaneously monitored. Data acquisition and processing were performed with the software (MassLynx, version 4.0; Waters).

2.2.3. Sample Preparation by FF-PPT

For a chromatographic assay, the preparation of complex biological matrices (e.g., rat plasma) is often involved and, as a result, the complicated processing protocol is frequently a limiting factor in the throughput of the assay. A fast flow protein precipitation (FF-PPT) method (Mallet et al., 2003; Rouan et al., 2001; Walter et al., 2001) was recently reported to facilitate the processing of complex biological matrices such as plasma samples in analytical procedures.

An aliquot (i.e., 45 μL) of the plasma sample was transferred to a protein precipitation filter (Unifilter FF-PPT; Whatman, Florham Park, NJ, USA). An aliquot (i.e., 5 μL) of the working internal standard solution (concentration of 1000 ng/mL, see section 2.2.4) was then added to the sample using an eight-channel pipette, and the plate vortexed for a few seconds. Approximately 200 μL of acetonitrile was dispensed to each well of the filter plate and mixed for 2 min using a plate vortexer. The Whatman Unifilter was placed on top of a vacuum manifold and a 96-well collection plate was placed at the bottom of the manifold. A reduced pressure of 18 inches of Hg was applied until all of the wells were cleared. The collection plate was then placed on an autosampler rack held at 4°C. A 5 μL aliquot from each well was injected on to the HPLC system.

2.2.4. Standards and Quality Control (QC) Samples

Stock solutions of LB and the IS were prepared in acetonitrile at concentrations of 1000 μg/mL and 1 μg/mL, respectively. A set of LB standard solutions and QC solutions were obtained by a successive dilution of the stock solutions with acetonitrile. The IS working solution was prepared daily in acetonitrile. A 5 μL aliquot of LB standard solution was spiked to 45 μL of blank rat plasma, resulting in eight nonzero calibration standards, to give concentrations of LB at 50, 100, 250, 500, 1000, 2500, 5000, or 10000 ng/mL. The QC samples was prepared to give concentrations of LB of 50, 150, 1000, or 8000 ng/mL of rat plasma. The samples were then processed similar to the procedure described in section 2.2.3.

2.2.5. Method Validation

2.2.5.1. Selectivity

The selectivity of the analysis was evaluated, using six lots of blank matrices (i.e., samples without LB and IS), of zero samples (i.e., blank plasma added with the IS), and of the lower limit of quantification (LLOQ) samples, for the presence of any interfering peak in the chromatograms.

2.2.5.2. Linearity

Calibration curves were constructed with the ratios of the peak area of LB to that of the IS against the LB concentration in the plasma standards. A series

of linear regression analyses were carried out assuming with or without the intercept, and weighing factor (1/x, $1/x^2$ or none). A preliminary experiment indicated that the model having a weighing of 1/x with an intercept provided the best fit (i.e., the smallest sums of square value) for the data. In subsequent studies, the best-fit model was used throughout the study.

2.2.5.3. Precision, Accuracy and Dilution

Three batches were used to assess the precision and accuracy of the assay. In the validation study, each batch, consisting of a set of six replicates of QC samples in a single run, was processed on separate days. The precision of the assay was estimated by the relative standard deviation at each concentration level. The accuracy of the assay was determined by calculating the difference between the calculated and theoretical concentrations. In addition, another batch with six replicates of the plasma samples containing 80000 ng/mL was prepared. The samples were then diluted tenfold with blank rat plasma to obtain an expected concentration at 8000 ng/mL. The diluted samples were then processed and analyzed to assess the concentration of the original sample adequately.

2.2.5.4. Matrix Effect and Recovery

The recovery and matrix effect were also determined in this study. The absolute/relative matrix effect and recoveries of LB and rosiglitazone were

assessed by analyzing three sets of standards at three concentrations (i.e., 150, 1000 and 8000 ng/mL). To determine the absolute matrix effect for LB and rosiglitazone, blank plasma, obtained from six rats, were extracted as described previously, and LB and rosiglitazone were added to the post-extraction sample to have three concentration levels (set 2). The mean peak areas of the analyte were compared with the mean peak areas from the neat solutions of the analyte in acetonitrile (set 1). For the case of the relative matrix effect, the variability, expressed as precision (CV,%), in the peak areas of the analyte added to the post-extraction samples from the blank plasma of six different rats (set 2) was determined and considered as the relative matrix effect (Matuszewski et al., 2003).

Recoveries of LB and rosiglitazone were determined by comparing the mean peak areas of analytes added before extraction into the six multiple sources as set 2 (set 3) with those of the analytes added post-extraction samples from multiple lots of rat plasma at three concentrations (set 2).

2.2.5.5. Stability

To evaluate the stability of the stock solution, a set of stock solutions for LB was freshly prepared and the response from the LC-MS/MS in fresh solutions compared with that from the stored stock solution. In this study, two storage conditions [i.e., a 6 h storage at room temperature (20°C) and a 3-week storage under refrigeration] were used. In addition, the stability of LB after

three cycles of the freeze-thaw process was evaluated. Thus, QC samples at 150 and 8000 ng/mL were freshly prepared, frozen at –80°C and, and the samples were then thawed at room temperature. The samples were then subjected to two additional cycles of the freeze-thaw process (i.e., total of three cycle). After the third thaw step, the samples were analyzed. Additionally, the post-preparative stability of processed samples in the autosampler (i.e., operating at 4°C) was assessed to determine whether an occasional delay in the analysis could lead to instability of the analyte. Short-term (bench-top) stability was determined by allowing the QC samples to stand on the bench-top for 24 h prior to the analysis. Long-term stability of the analyte in rat plasma at –80°C was evaluated by analyzing QC samples over a time course of 2 weeks. In the stability assessment studies (i.e., stock solution stability, freeze-thaw stability, post-preparative stability and short-/long-term stability), the analyte was considered stable if the difference in the response was less than 15% from that in the corresponding fresh sample (in the case of the stock solution stability) or in the concentration from the theoretical value (in the case of other stability studies).

2.2.6. Application of the Assay

To determine the applicability of the assay to pharmacokinetic studies involving LB, the compound was orally administered to female rats and the assay was used to determine its concentration in plasma samples. Female

Sprague-Dawley rats, weighing 125.0 to 139.8 g (i.e., 5 weeks of age) were used in this study. LB was dispersed in a 5% gum arabic solution and the solution administered orally at a dose of 1 mg/kg. Blood samples (0.25 mL) were collected into heparinized tubes via the tail vein prior to and at 0.5, 1, 2, 3, 4, 8, and 24 h after administration of the drug. Plasma samples, obtained by centrifugation of the blood at 16100 g for 5 min, were stored at –80°C prior to analysis. Experimental protocols involving animals in this study were reviewed by the Institutional Animal Care and Use Committee (IACUC) of the Korea Institute of Toxicology, according to National Institutes of Health guidelines (NIH publication number 85-23, revised 1985) “Principles of Laboratory Animal Care”. All animals used in this study were cared for in accordance with the principles outlined in the NIH publication of "Guide for the Care and Use of Laboratory Animals".

The maximum LB concentration (C_{max}) and the time to reach C_{max} (T_{max}) were read directly from the temporal profile of LB concentration in the plasma. When it was necessary to determine the pharmacokinetic parameters, the standard moment analysis was used. The area under the LB concentration in the plasma-time curve from time zero to infinity (AUC_{inf}) and the area under the respective first moment-time curve from time zero to infinity ($AUMC_{inf}$) were calculated by linear trapezoidal method and appropriate area

extrapolation (Gibaldi and Perrier, 1982). MRT, the mean residence time, was estimated using by the equation below;

$$\text{MRT} = \frac{AUMC_{inf}}{AUC_{inf}}$$

The terminal phase half-life ($t_{1/2}$) was calculated from the slope (λ) of the log-linear portion of the concentration time profile using the equation below;

$$t_{1/2} = \frac{0.693}{\lambda}$$

2.3. *In vitro* Absorption, Distribution and Elimination Studies

2.3.1. Parallel Artificial Membrane Permeability Assay (PAMPA)

To estimate the intestinal permeability of LB via diffusional transport, PAMPA was carried out following the standard procedure (Kerns et al., 2004; Zhu et al., 2002). Briefly, a dodecane solution containing phosphatidylcholine (20 mg/mL) was added to the membrane (multiscreen PAMPA assay plate, #MAIP-N4550) of the insert. Phosphate buffered saline containing LB (200 μg/mL) in 15% DMSO and 15% PEG 400, or LB sulfate (100 μg/mL) in 10% DMSO, was added to the well before the artificial membrane material had evaporated (<10 min). The reaction was initiated by inserting the donor plate into the acceptor plate, and allowing the process to proceed at room

temperature. When necessary, the permeability of verapamil (i.e., the high permeability marker for this assay) was measured in parallel. The acceptor buffer was collected at 16 h after the initiation and the concentration was measured using an HPLC-UV spectrophotometer (e2695, 2489; Waters). The mobile phase involved the isocratic condition of 0.1% formic acid-acetonitrile (70:30, v/v) at a flow rate of 1 mL/min at 25°C. After 50 μL of samples were injected onto a reversed phase HPLC column (Kinetex XB-C18, 150 mm × 4.6 mm, 5 μm; Phenomenex, Torrance, CA, USA), the eluent from the column was monitored at a wavelength of 290 nm. The apparent permeability of each compound was calculated using the standard equation (Zhu et al., 2002).

2.3.2. Permeability Study in MDCK II Cells

MDCKII-WT and MDCKII-MDR1 cell lines were generously provided by Dr. Borst (The Netherlands Cancer Institute, Amsterdam, Netherlands). Cells were cultured in DMEM (Welgene Inc., Daegu, Korea) containing 10% fetal bovine serum (FBS, Welgene Inc.), 1% non-essential amino acid solution, 100 units/mL penicillin, and 0.1 mg/mL streptomycin under a humidified atmosphere of air containing 5% CO_2 at 37°C. A collagen-coated 12 mm Transwell (Costar; Corning, NY, USA) was incubated with medium at 37°C for 1 h to improve cell attachment. Cells were seeded at a density of 2.5×10^5 cells/well and the medium was replaced at 2 day intervals. Bidirectional transport experiments were performed on 5 days after seeding. The

confluence of the cell monolayer and integrity of tight junctions were confirmed by microscopy and the measurement of transepithelial electrical resistance (TEER, 130-180 Ω), respectively. Apical or basolateral chambers were washed twice and preincubated with the transport buffer [25 mM HEPES, 140 mM NaCl, 5.4 mM KCl, 1.8 mM $CaCl_2$, 0.8 mM $MgSO_4$ and 5 mM glucose (pH7.4)] at 37°C for 30 min.

For the inhibition study, the basolateral to apical transport of LB was measured in the presence and absence of verapamil (i.e., inhibitor). In this assay, cells were preincubated with the transport buffer containing verapamil (500 μM) for 15 min. Transport buffer containing only LB (i.e., 5 μM) or LB with the inhibitor was added to the donor chamber (500 μL for the apical chamber and 1.5 mL for the basolateral chamber), the drug-free transport buffer was placed in the receiver chamber, and the cells were incubated at 37°C. The final concentration of the organic solvent (e.g., DMSO) in the transport buffer was below 1% in all of the experiments. Aliquots were collected from the receiver chamber at 30, 60, 90, and 120 min and the solution was replenished with the same volume of fresh transport buffer. Samples were stored at –80°C until analysis. LB was quantified using LC-MS/MS (Lee et al., 2009). The apparent permeability coefficient (P_{app}, cm/sec) was calculated using the equation below:

$$P_{app} = \frac{\mathrm{dQ}}{\mathrm{dt}} \times \frac{1}{A} \times \frac{1}{C_0}$$

where dQ/dt is the transport rate, A is the surface area of the membrane, and C_o is the initial concentration of the test compound on the donor side. When necessary, the net efflux ratio was also determined using the equation below, the apparent permeability from the basolateral-to-apical direction ($P_{app,\ B\ to\ A}$) and the apparent permeability from the apical-to-basolateral direction ($P_{app,\ A\ to\ B}$):

$$\text{Efflux ratio} = \frac{P_{app,\ B\ to\ A}}{P_{app,\ A\ to\ B}}$$

2.3.3. Interaction of LB with Carrier-mediated Transports in MDCK Cells Expressing OATP1B1, OATP1B3, OAT1, OAT3, OCT2 and BCRP

To determine the interaction of LB with major transporters, organic anion transporting polypeptide 1B1 (OATP1B1), OATP1B3, organic anion transporter 1 (OAT1), OAT3 and organic cation transporter 2 (OCT2) were cloned and functionally expressed in MDCK cells containing the Flip-In system (Invitrogen, Carlsbad, CA, USA) described in section 3.2.4. In addition, MDCKII-BCRP cells, generously provided by Dr. Borst in the Netherland Cancer Institute, were also used. Cells were typically cultured in DMEM (Hyclone Lab, Thermo Scientific, Rockford, IL, USA) containing 10%

fetal bovine serum, 1% non-essential amino acids, 100 units/mL penicillin, 0.1 mg/mL streptomycin, 40 μg/mL gentamicin and 10 mM HEPES under an atmosphere of 5% CO_2 and 90% humidity.

To determine whether LB interacts with one or more of the uptake transporters, the cells expressing the transporters were seeded at the density of 5×10^5 cells/well in 24 well plates. After 2 days, the cells were washed twice and pre-incubated with Hank's balanced salts solution, 25 mM HEPES and 25 mM glucose (pH 7.4). The cells were then incubated for 10 min at 37°C with the buffer medium containing 1 μM of radiolabeled substrates [i.e., [^{3}H] p-aminohippuric acid (OAT1), [^{3}H] estrone-3-sulfate (OAT3) [^{3}H] estradiol-17β-glucuronide (OATP1B1, OATP1B3) and [^{3}H] 1-methyl-4-phenylpyridinium (OCT2)] in the absence and presence of varying concentrations of LB. Upon completion of the incubation (i.e., 10 min), the medium was removed, and the cells were washed three times with ice-cold Dulbecco's phosphate-buffered saline, followed by solubilization in 0.2 N NaOH. The amount of substrate accumulated by the cell was determined by liquid scintillation counter (Tri-Carb 3110 TR; Perkin-Elmer Life Science, Boston, MA, USA) and were normalized relative to the cell lysate protein concentration determined (Ueki et al., 2006). The cellular accumulation was plotted against the LB concentration and the concentration resulting in the 50%

inhibition (IC_{50}) value was estimated by nonlinear regression analysis using the following equation:

$$V = V_{max} \times \frac{1 - C}{C - IC_{50}}$$

where V is transport rate in percentage of control, V_{max} is the maximum reaction velocity, and C is concentration of LB.

For the case of BCRP mediated transport, MDCKII-BCRP cells were seeded on collagen-coated Transwell (Corning ct# 3493) inserts at a density of 2.5×10^5 cells/insert and were grown for 5 days (Li and Au, 2001). The integrity of the cell monolayer was evaluated prior to the transport experiments by measuring the TEER value. Cell monolayers were considered intact and suitable for use in transport experiments when the value was more than 150-180 Ω·cm (Hanefeld, 2001; Soldner et al., 2000). Prior to the transport experiments, cell monolayers were washed twice and preincubated with a buffer comprising a Hank's balanced salts solution, 25 mM HEPES, and 25 mM glucose (pH 7.4). After washing, the plates were incubated in the buffer medium for 30 min at 37°C, and then TEER values were measured (Li and Au, 2001). For the transport experiment, 1.5 mL of buffer medium containing [^{3}H]-methotrexate in the presence and absence of 100 μM LB was added to the basolateral side, and 0.5 mL of buffer medium was added to the apical side. A 0.3-mL aliquot of buffer medium was taken from the apical side

and replaced with fresh medium every 30 min for 2 h. The amount of radiolabeled methotrexate transport through the cell monolayer was determined by the liquid scintillation counter (Tri-Carb 3110 TR; Perkin-Elmer Life Science).

2.3.4. Estimation of IC_{50} of LB on Digoxin Efflux in MDCKII Cells Expressing MDR1

To investigate the reason(s) underlying the discrepancy between the bioavailability estimation from the PAMPA and cell permeability assay, a transport study of the compound that had been accumulated in cells grown on a solid support, rather than vectorial transport (Li and Au, 2001), was performed. However, during the preliminary experiment, MDCKII-MDR1 cells were found to be inappropriate because changes in cellular accumulation were not readily detected in the presence of the substrate or inhibitor, probably because of insufficient expression of the efflux transporter. Therefore, a human MDR1 clone was obtained, sub-cloned into the pcDNA5/FRT vector (Invitrogen) and functionally expressed in MDCK-Flip-in cells (described in section 3.2.4.). To determine the apparent affinity of LB to MDR1, MDCK-Flip-in-MDR1 cells were seeded at the density of 5×10^5 cells/well in 24-well plates. After 2 days, the cells were washed twice and pre-incubated with a buffer comprising Hank's balanced salts solution, 25 mM HEPES and 25 mM glucose (pH 7.4). Next, cells were incubated for 10

min at 37°C with the buffer medium containing 1 μM [^{3}H] digoxin in the absence and presence of varying concentrations of LB. Upon the completion of incubation (i.e., 10 min), the medium was removed and washed three times with ice-cold Dulbecco's phosphate buffered saline, followed by solubilization in 0.2 N NaOH. The amount of substrate that had accumulated within the cell was determined by the liquid scintillation counter (Tri-Carb 3110 TR; Perkin-Elmer Life Science) and was normalized to the amount of lysate protein used in the reaction. The percent inhibition was plotted against the LB concentration and IC_{50} estimated by nonlinear regression analysis using the following equation:

$$V = V_0 + (V_{max} - V_0) \times \frac{C}{C + IC_{50}}$$

where V is transport rate percent of the control, V_{max} is the maximum reaction velocity, V_0 is the basolateral transport rate as a percent of the control, and C is the concentration of LB.

2.3.5. Determination of Plasma Protein Binding and the Blood-Plasma Partitioning of LB

The extent of LB binding to rat plasma proteins was estimated at 37°C using an ultrafiltration method. Rat plasma samples were spiked with LB to have the final concentrations of 0.1, 0.5 and 2.5 μg/mL, respectively (in triplicate). After pre-incubation at 37°C for 30 min, an aliquot (0.4 mL) was transferred

to an Amicon Microcon Centrifugal Filter Devices (30000 DA cut-off YM-30; Millipore, Bedford, MA, USA). The device was centrifuged at 2300 g for 20 min at 37°C to obtain the ultrafiltrates. The concentration of LB in the filtrate was then determined by LC-MS/MS. The unbound fraction of LB in the plasma was determined from the ratio of the ultrafiltrate concentration to plasma concentration.

To determine non-specific binding to the ultrafiltration device, LB was added to water at concentrations of 0.1, 0.5 and 2.5 μg/mL, and an aliquot (0.4 mL) was transferred/centrifuged at 2300 g for 20 min. Nonspecific binding was determined by comparing the chromatographic peak area ratios for LB in water before and after the ultrafiltration procedure.

When necessary, the extent of protein binding was also determined by a rapid equilibrium dialysis method. According to the manufacturer's protocol (Thermo scientific, Waltham, MA, USA), LB was added to an aliquot of rat plasma at a final concentration of 2.5 μg/mL and the base plate of the rapid equilibrium dialysis device was then rinsed with 20% ethanol for 10 min. An aliquot of the plasma (100 μL) and PBS (300 μL) were placed into the sample chamber and the buffer chamber, respectively, and the RED device was covered/incubated on a shaker at 37°C for 4 h. After the incubation, a 50 μL aliquot was collected from each side of the chamber. A 50 μL portion of blank plasma was then added to buffer sample, and an equal volume of PBS was

also added to the plasma samples to adjust for matrix effects. A 200 μL aliquot of acetonitrile containing the internal standard was added to each sample, and supernatants were obtained by centrifugation at 4°C for 20 min at 3200 g for use in the LC-MS/MS analysis. The fraction of unbound LB in the plasma was determined by dividing the LB concentration in the buffer compartment by that in the plasma compartment.

The blood/plasma concentration ratio of LB was also determined in fresh rat blood. LB in DMSO was added to blank blood and was diluted with the blood to obtain a final LB concentration of 0.1 and 2.5 μg/mL. Blood was then incubated at 37°C in a shaking water bath for 30 min. After incubation, the plasma was separated from whole blood by centrifugation. Control samples containing LB in the rat plasma were prepared to a final concentration of 0.1 and 2.5 μg/mL. The blood/plasma concentration ratio was calculated from the concentration difference between the control plasma and plasma isolated from whole blood.

2.3.6. Liver Microsomal Stability

The time-dependent metabolic stability of LB in rat liver microsomes was determined. The reaction mixture (total volume of 0.47 mL) consisted of rat liver microsomes (Corning Gentest, Tewksbury, MA, USA) in 100 mM potassium phosphate buffer (pH 7.4) and LB (10 μM, final concentration). After preincubation at 37°C for 5 min, the reaction was initiated by the

addition of an NADPH-regenerating solution (Corning Gentest). Samples (50 µL) were collected at 0, 1, 3, 5, 15, and 30 min. The reaction was terminated by adding 150 µL of ice-cold acetonitrile containing rosiglitazone (100 ng/mL, internal standard). After mixing by vortexing and subsequent centrifugation at 4°C for 5 min at 15700 g, the clear supernatant was collected and analyzed by LC-MS/MS for the quantification of LB.

When necessary, the rate of glucuronidation was determined for LB in the presence of UDP-glucuronic acid under similar reaction conditions and procedures, except that UDP-glucuronosyltransferase (UGT) was added to the reaction mixture (Corning Gentest), in place of the NADPH regenerating solution. Samples (50 µL) were collected at 0, 2, 5, 10, 15, and 30 min of the reaction. Testosterone (final concentration 20 µM) and 7-hydroxycoumarine (final concentration 1 µM) were used as positive controls for the oxidation and glucuronidation reactions, respectively. The *in vitro* metabolic half-life was calculated using the slope (k), obtained from linear regression analysis, of the remaining concentration of LB versus time (Obach et al., 1997).

$$t_{1/2} = -\frac{\ln 2}{\mathrm{k}}$$

2.3.7. Cytochrome P450 Inhibition Study

The potential of LB to inhibit major human CYP enzymes was evaluated using human liver microsomes (XenoTech, LLC; Lenexa, KS, USA). The

reaction mixture comprising of 1 mg/mL human liver microsomes, 10 mM $MgCl_2$, 10 μM LB and the control in pH 7.4 potassium phosphate buffer was prepared (total volume 360 μL) and equilibrated at 37.5°C for 5 min. The reaction was initiated by the addition of 1 mM NADPH and the substrate [i.e., phenacetin (CYP1A2), tolbutamide (CYP2C9), S-mephenytoin (CYP2C19), dextromethorphan (CYP2D6), nifedipine (CYP3A4) and testosterone (CYP3A4)] of CYPs (final concentrations of 100, 10, 100, 10, 5 and 50 μM for 1A2, 2C9, 2C19, 2D6 or 3A4, respectively); the mixtures were then incubated in a shaking water bath at 37.5°C for 30 min. Aliquots (100 μL) were withdrawn in triplicate at 30 min, and 100 μL of ice-cold acetonitrile-water (50:50, v/v) were added to terminate the reaction. The samples were vortexed briefly and centrifuged at 9300 g for 10 min, and the supernatant from each sample was collected. The concentration of LB in the supernatant was then measured using LC-MS/MS.

All of the analyses were performed using an LC-MS/MS system interfaced with an Agilent 1100 HPLC and an AB/SCIEX 3200 QTRAP (Applied Biosystems, Foster City, CA, USA). Chromatographic separation was performed using an HPLC column (SB-Aq, 2.1 mm × 50 mm, 3.5 μm, Zorbax; Agilent, Santa Clara, CA, USA). The mobile phase consisted of solvent A, 0.1% formic acid in water, and solvent B, acetonitrile, with an A/B gradient for the metabolite [i.e., acetaminophen (CYP1A2), 4-OH

tolbutamide (CYP2C9), 4-OH mephenytoin (CYP2C19), dextrophan (CYP2D6), 4-OH nifedipine (CYP3A4) and 6-OH testosterone (CYP3A4)] of the substrate with a flow rate of 0.3 mL/min. In the present study, MRM *m/z* transitions at 152→109 (acetaminophen), 287→135 (4-OH tolbutamide), 235→150 (4-OH mephenytoin), 258→157 (dextrophan), 345→284 (4-OH nifedipine) and 305→91 (6-OH testosterone) were simultaneously monitored. Data acquisition and processing were performed using the software (Analyst, version 1.4.2; Applied Biosystems).

The % inhibition can be calculated as follows:

$$\%\ inhibition = \frac{Peak\ area\ without\ inhibitor - peak\ area\ with\ inhibitor}{Peak\ area\ without\ inhibitor} \times 100$$

2.3.8. Metabolite Identification of LB

LB was incubated with rat liver microsomes (Corning Gentest) in the presence of an NADPH regenerating system in 100 mM potassium phosphate buffer (pH 7.4). Stock solutions of test compounds were prepared in DMSO and added to the microsomal incubation with a final organic solvent concentration of under 1% (v/v). The initial incubation mixture consisting of LB, rat liver microsomes was pre-incubated for 5 min. The reaction was initiated by adding an NADPH generating system. Control samples were

incubated without NADPH. The final volume in incubation was 500 μL. The final concentrations of microsome and LB in the incubation mixture were 0.5 mg/mL and 100 μM, respectively. The incubation was terminated after 30 min by the addition of three times of ice-cold acetonitrile. After mixing by vortexing and subsequent centrifugation at 4˚C for 5 min at 16100 g to remove precipitated protein, and analyzed by liquid chromatography-tandem mass spectrometry.

LC-ESI-QTRAP system consisted of a Agilent 1100 series HPLC system (Santa Clara, CA) and an AB Sciex 3200 QTRAP hybrid triple quadrupole/linear ion trap mass spectrometer equipped with a Turbo V Ion Spray source operated in enhanced resolution (ER) scan mode, enhanced mass spectrum (EMS), enhanced product ion (EPI) mode, multiple reaction monitoring (MRM). Especially, EPI and MRM mode was used to identify structural information. The sample injection volume was 10 μL, and the separation was performed on a Waters Atlantis dC C18 column (2.1 mm × 100 mm, 3 μm; Waters, Milford, MA, USA) maintained at room temperature. The mobile phase consisted of A (methanol with 0.1% formic acid) and B (purified water with 0.1 % formic acid) and the flow rate was set at 0.25 mL/min with methanol-pure water (80:20, v/v) containing 0.1% formic acid. Source parameters were set as follows: curtain gas: 15 psi; positive ion source: 5500 V; source temperature: 500°C; nebulizer gas (GS 1): 45 psi; auxiliary

gas (GS 2): 55 psi; collision activated dissociation (CAD) gas: high; declustering potential and collision energy: varied dependent on scan.

General unknown screening was accomplished using an MS survey scan from m/z 100-900 to identify any major components in the rat liver microsome samples, including unexpected compounds. For optimal sensitivity, the EMS scan-type was used in the linear ion trap of the QTRAP system. Information Dependent Acquisition (IDA) criteria were employed in order to automatically trigger the acquisition of the EPI scan to acquire full-scan MS/MS spectra of metabolite ions predicted, since it provides improved data quality, better sensitivity, higher resolution, and faster acquisition. In addition, target screening was accomplished using a MRM scan to identify analytes, since MRM scans are extremely sensitive and selective, this survey scan to detect drugs presented at low concentrations in complex biological matrices.

The strongest MRM signal with ion counts higher than 5000 was selected by the IDA criteria, and the EPI scans were triggered to be collected for three consecutive scans then be excluded in the target for 30 sec. Internal standard (m/z 358.2) was excluded in the IDA exclusion list across the full LC run. The EPI scan was operated ranging from m/z 100 to 800 at a scan rate of 4000 amu/s with dynamic fill in the linear ion trap. The collision energy (CE) was set at 67 eV with a CE spread of 10 eV. Dynamic fill time function was used

to prevent overfilling of the linear ion trap (LIT). Data was processed using Analyst software 1.4.2 and Metabolite ID 1.3 (Applied Biosystems).

2.4. *In vivo* Pharmacokinetic Studies

2.4.1. Animals

Male *Sprague-Dawley* (SD) rats, 6-7 weeks old, were purchased from Orient Bio Inc. (Gyeonggi-do, Korea) and were used in all *in vivo* studies and in the collection of blank blood and tissue samples. Experimental protocols involving the animals used in this study were reviewed by the Seoul National University Institutional Animal Care and Use Committee according to the National Institutes of Health Publication Number 85-23 Principles of Laboratory Animal Care revised in 1985.

2.4.2. Administration to Rats

Male SD rats, weighing approximately 250-300 g, were anesthetized by an intramuscular administration of 50 mg/kg tiletamine HCl/zolazepam HCl (Zoletil 50; Virbac Laboratories, France) and 10 mg/kg xylazine HCl (Rompun; Byer Korea, Korea). After confirming the induction of anesthesia, the femoral artery (for collecting blood samples) and vein (for supplementing body fluids or administration) were catheterized with polyethylene tubing (PE 50; Clay Adams, Parsippany, NJ, USA), filled with heparinized saline (25 U/mL) and saline, respectively. The LB administration study was carried out after the confirmation of recovery from the anesthesia. For the intravenous administration study, solutions were injected via the intravenous catheter at the dose of 0.5, 1 or 2 mg/kg. For oral administration, the rats received LB at

a dose of 0.5 or 2 mg/kg via oral gavage. The vehicle for LB administration (both routes) was DMSO/PEG400/distilled water (0.5:4:5.5) (typical dosing volume of 2 mL/kg) throughout the pharmacokinetic study.

Blood samples (150 μL for each sample) were collected from the arterial catheter at pre-dose, 1, 5, 10, and 30 min and 1, 2, 4, and 8 h post-dosing (intravenous administration) or at pre-dose, 5, 10 and 30 min and 1, 2, 4, 8, and 12 h post-dosing (oral administration). Plasma was separated from the blood samples by centrifugation (16100 g, 5 min, 10°C) and stored at −70°C. Preliminary study indicated that blood sampling did not cause any effect on the hematocrit (i.e., hematocrit from the pre-dose blood sample = 46.8 ± 2.2%; the hematocrit from after the 11^{th} sampling = 42.6 ± 1.6%; not significant).

When it was necessary to determine the biliary recovery of LB, the bile duct of the rat was catheterized. Male SD rats were anesthetized and catheterized following a procedure similar to that described above, except that the bile duct was catheterized with polyethylene tubing (PE 10; Clay Adams). After recovering from the anesthesia, the rats were intravenously administered with LB at an intravenous dose of 0.5 or 1 mg/kg, and the bile was collected at designated time intervals (0–2, 2–4, 4–6, 6–8, and 8–24 h). The bile samples were weighed and stored at −80°C until the analysis. Pooled urine and gastrointestinal (GI) tract samples were also collected. Male SD rats were injected with LB via the tail vein at a dose of 0.5, 1 or 2 mg/kg and were

placed in metabolism cages with free access to water. Urine samples were collected in tubes on dry ice at designated time intervals (0–8, and 8–24 h) after intravenous administration. The metabolic cage was rinsed with 10 mL of distilled water at 8 and 24 h. After measuring the exact volume of the combined urine sample, the samples were stored in a –80°C freezer until the analysis. To determine the fraction of LB remaining in the intestine, the entire gastrointestinal tract, including its contents and feces, was removed at 24 h after the oral and intravenous administration, transferred into a beaker containing 100 mL of methanol to facilitate the extraction of LB, cut into small pieces using scissors, and then homogenized using a PowerGen 1000 Homogenizer (Fisher Scientific Inc., Waltham, MA, USA) and stored at –70°C until the analysis.

2.4.3. Tissue Distribution Studies

LB at a dose of 2 mg/kg was administered intravenously over 1 min to SD male rats via the tail vein. The rats were sacrificed with CO_2 at 1 h after the administration, and blood samples were collected. In addition, approximately 1 g each of tissue from the brain, liver, lung, heart, small intestine, large intestine, kidney, spleen, fat, testis, or muscle was excised immediately. The tissues were added to six volumes of a mixture (acetonitrile:water = 1:1, v/v) per tissue weight, homogenized using a PowerGen 1000 Homogenizer (Fisher Scientific Inc.), and stored at –70°C until the analysis.

2.4.4. Data Analysis

Standard moment analysis was carried out to calculate the pharmacokinetic parameters (Gibaldi and Perrier, 1982), including the area under the plasma concentration-time curve (AUC), first moment of plasma concentration-time curve (AUMC), time-averaged total body (CL), renal (CL_r)/nonrenal (CL_{nr}) clearances, $t_{1/2}$, MRT, apparent volume of distribution at steady state (V_{ss}), and extent of absolute oral bioavailability (F). In this analysis, the area until the last sampling time was calculated by the linear trapezoidal method added to the remaining area to the infinite time calculated by standard methods. The C_{max} and T_{max} after oral administration were directly read from the concentration-time profile.

When it was necessary to compare the means between the treatments, Student's t-test or one-way ANOVA, followed by Duncan's test, was typically used. Data are expressed as the mean ± standard deviation (S.D.).

2.5. Gender Differences in the Hepatic Elimination and Pharmacokinetics of LB in Rats

2.5.1. Animals

Male and female Sprague-Dawley rats were purchased from Orient Bio Inc. (Gyeonggi-do, Korea). The experimental protocols involving animals in this study were reviewed by the Institutional Animal Care and Use Committee

(IACUC), according to National Institutes of Health guidelines (NIH publication number 85-23, revised 1985) “Principles of Laboratory Animal Care”. All animals used in this study were cared for in accordance with the principles outlined in the NIH publication of "Guide for the Care and Use of Laboratory Animals".

2.5.2. LB Pharmacokinetic Studies

LB was dispersed in 5% gum arabic solutions at concentrations of 0.02, 0.2, and 2 mg/mL. The suspension was administrated orally to rats (body weight 108-142 g, 5 weeks of age) at doses of 0.1, 1, and 10 mg/kg via oral gavage. Blood samples (0.25 mL) were collected in heparinized tubes via the tail vein at pre-dose, 0.5, 1, 2, 3, 4, 8, and 24 h post-dosing. Plasma was separated from the blood samples by centrifugation (16100 g, 5 min, 10°C) and stored at –80°C until the analysis. The concentration in the plasma sample was determined by a previously described method (Lee et al., 2009).

When it was necessary to compare the bound fraction of LB to male or female rat plasma proteins, a RED method was used. In this study, the total LB concentration was set at 1 μM, and protein binding was determined according to the manufacturer’s protocol (Thermo Scientific, Waltham, MA, USA). The concentration of LB in samples collected from each side of the chamber was determined by a procedure described previously (Lee et al., 2009), and the percent bound calculated by the following equation:

$$\% \text{ Bound} = (1 - \frac{C_{buffer}}{C_{plasma}}) \times 100$$

2.5.3. Stability of LB in Incubations Containing Male or Female Rat Liver Microsomes

In this study, the metabolic stability of LB was assessed and compared in incubations of LB with liver microsomes obtained from male or female rats. Regardless of the source of the microsomes, the reaction mixture consisted of rat liver microsomes (Corning Gentest, 0.5 mg protein/mL, final concentration) in 100 mM potassium phosphate buffer (pH 7.4) and LB (10 μM, final concentration) along with an NADPH-regenerating solution (Corning Gentest). The remaining concentration of LB in the microsomal incubation was determined at 0, 2, 5, 10, 15, 30 and 60 min after the initiation of the reaction by LB assay (Lee et al., 2009).

The *in vitro* metabolic stability parameters for males and females were estimated in this study. Thus, the slop (K) of the natural log of the percentage of remaining LB in the incubation-time plot was estimated using a linear regression analysis and the half-life ($t_{1/2}$) for the microsomal incubation calculated by the following equation (Baranczewski et al., 2006; Chaturvedi et al., 2001; Huang et al., 2010; Pang and Rowland, 1977).

$$t_{1/2} = \frac{0.693}{K}$$

The estimated *in vitro* microsomal intrinsic clearance (CL_{int}) in rat liver microsomes was also estimated by normalizing the rate to the amount of microsomal protein (mg/mL) as follows:

$$\mathrm{CL_{int}\ (mL/min/mg\ protein)} = \frac{0.693}{t_{1/2}} \times \frac{\mathrm{mL\ incubation}}{\mathrm{mg\ microsomes}}$$

2.5.4. Pharmacokinetic and Statistical Analyses

The C_{max} and T_{max} were directly read from the experimental data. The area under the plasma concentration-time curve from time zero to the last quantifiable time point (AUC_{last}) was calculated by the linear trapezoidal rule using WinNonlin (version 5.2.1, Pharsight Corporation, Mountain View, CA, USA) (Gibaldi and Perrier, 1982). Other pharmacokinetic parameters were calculated by standard methods (Gibaldi and Perrier, 1982). Data are expressed as the mean values ± the standard deviation (S.D.). For the comparison of means, unpaired t-test was used. A p value less than 0.05 ($p<0.05$) was considered as denoting statistical significance.

3. RESULTS

3.1. Quantification of LB in Rat Plasma Using a Liquid-Chromatography/Tandem Mass Spectrometry

3.1.1. Chromatography

The chemical structures of LB and rosiglitazone (i.e., the IS) are shown in Fig. 1. Preliminary studies, involving the adjustment of the collision energy and cone voltage, indicate that the transition conditions of *m/z* 482→258 (for LB) and *m/z* 358→135 (for IS) are adequate for its detection and the quantification. Results from preliminary study, indicates that the concentrations of metabolites, having the *m/z* values (i.e., 218, 231, 467), accounted for significantly less (i.e., approximately 12.5%) than that of the parent drug at various times up to 4 h. In addition, these metabolites do not appear to possess pharmacological activities. Therefore, these analytical conditions were used in subsequent studies.

Preliminary studies were also carried out to optimize the selectivity as well as the throughput of the assay by adjusting the chromatographic conditions. As a result, the chromatographic condition with retention times of 1.3 min for LB and 2.6 min for the IS was found to be adequate with

apparently symmetric peaks for both LB and the IS (Fig. 2). These chromatographic conditions were used in subsequent studies

3.1.2. Specificity and Lower Limit of Quantification

Under the LC-MS/MS conditions used, LB and the IS were clearly separated from endogenous peaks originating from the blank matrix (Fig. 2). Similarly, chromatograms of six lots of blank analyses indicate that the analyte peaks were well separated from interfering peaks (Fig. 2 and Table 1) and that the assay condition has an adequate specificity for LB. At the lowest concentration level (i.e., 50 ng/mL) of LB, the accuracy (RE) and precision (CV) for the six replicates were –7.20% and 1.31%, respectively (Table 3). Furthermore, the signal to noise level was at least 33 at this concentration. Taking the above data into consideration, the lower limit of the quantification was determined at 50 ng/mL for this assay.

(a)

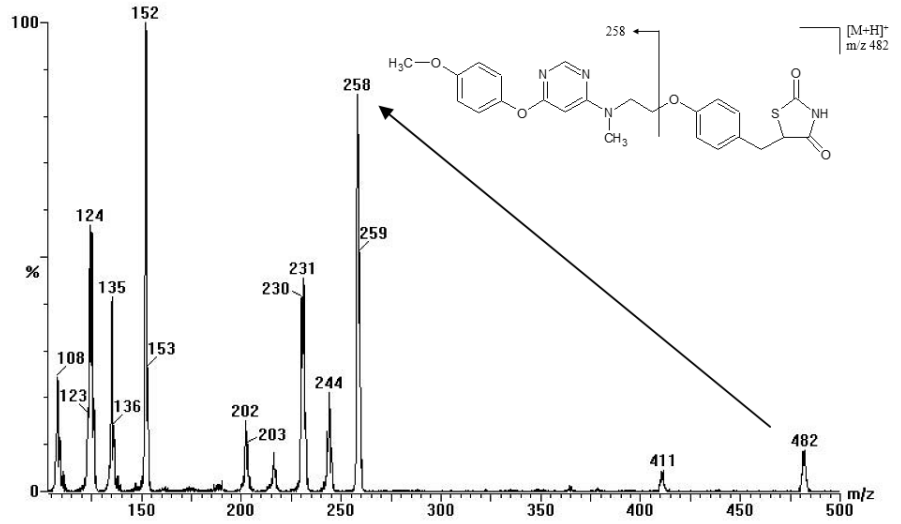

(b)

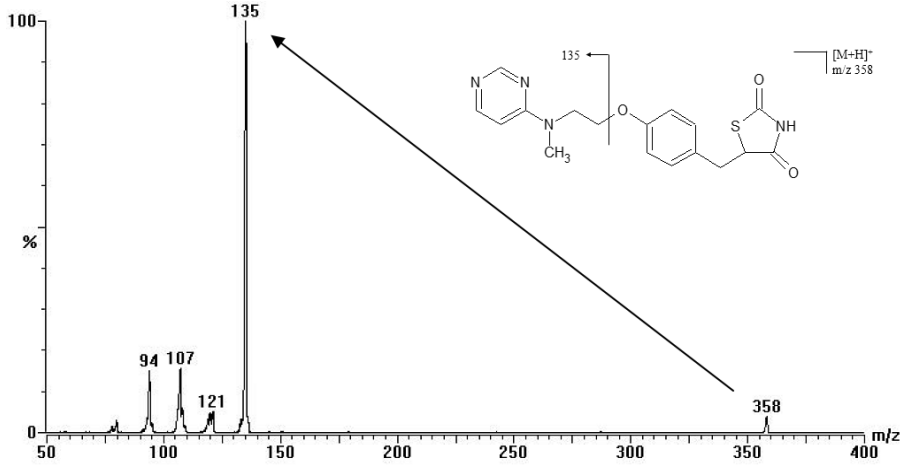

Figure 1. The structures and product-ion scan spectra of (a) LB and (b) rosiglitazone (i.e., the internal standard).

(a)

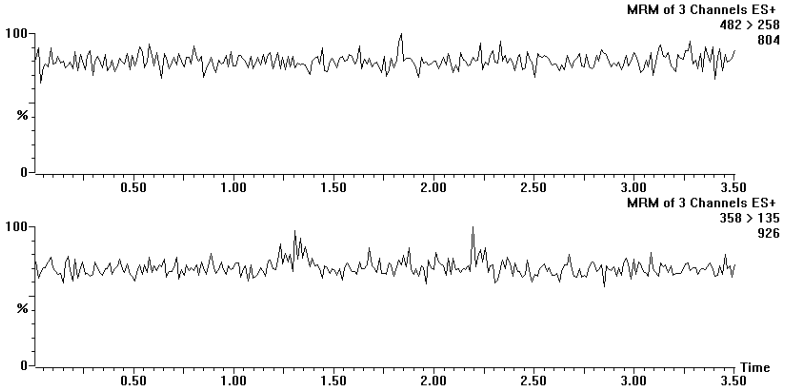

(b)

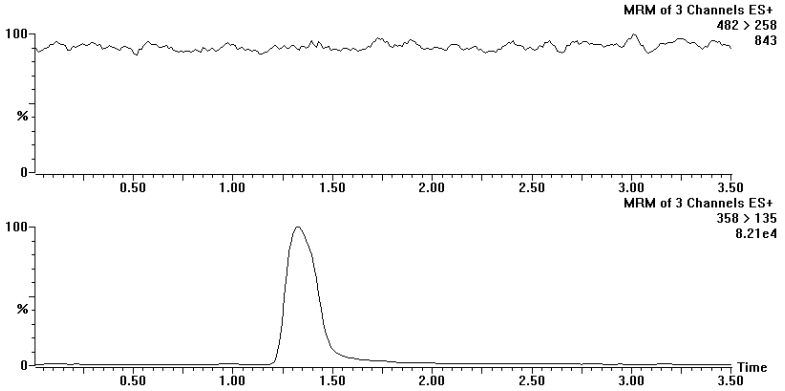

(c)

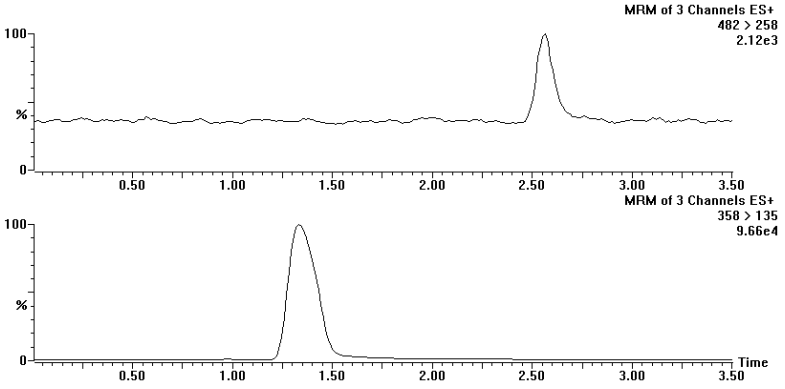

Figure 2. Multiple reaction monitoring (MRM) chromatography of (a) double blank plasma, (b) plasma containing rosiglitazone (IS, 1000 ng/mL), (c) plasma containing LB at LLOQ (50 ng/mL) and IS.

3.1.3. Linearity

The calibration curves for LB in rat plasma appeared to be linear over the concentration range of 50-10000 ng/mL. A linear regression analysis of the data indicated that the correlation coefficient was in excess of 0.999 for three batches of calibration curves. Table 2 shows the results of a statistical analysis obtained from three runs of calibration curve for LB.

3.1.4. Accuracy, Precision, and Sample Dilution

QC samples, having four concentration levels (50, 150, 1000, and 8000 ng/mL), were analyzed in six replicates to determine the intra-day accuracy and precision, and the accuracy (RE) for LB ranged from –7.20 to 5.65% with a precision (CV) of between 1.31 and 5.74% (Table 3). In addition, the inter-day accuracy and precision were estimated using six QC replicates at the four concentration levels on 3 different days. The accuracy (RE) for LB ranged from –5.33 to 1.70% with a precision (CV) of between 3.97 and 5.05% (Table 3).

In pharmacokinetic studies, the concentrations of analyte in certain plasma samples may exceed the upper limit of quantification set by the assay. Therefore, an adequate assay should be capable of properly estimating the concentration of such samples by appropriate dilution and correction. To demonstrate the versatility of the current assay, a set of plasma samples was prepared so as to contain a LB concentration of 80000 ng/mL (viz, the upper

limit of quantification to be 10000 ng/mL in this assay). The samples were then diluted tenfold to give the expected concentration of LB of 8000 ng/mL and analyzed. As shown in Table 3, the calculated concentration was found to be 7920 ng/mL (i.e., the percent deviation from the theoretical value of –0.957%) with a CV of 1.88%, suggesting that the assay is capable of reasonably estimating LB concentrations in samples that exceed the upper limit by appropriate dilution.

Table 1. Specificity of LB measurements in rat plasma.

Matrix Lot.	Response (Peak area)			
	Blank[a)]	Zero Blank[b)]	LLOQ[c)] (50 ng/mL)	HQC[d)] (8000 ng/mL)
1	0.00	0.00	153	18300
2	0.00	0.00	143	18900
3	0.00	0.00	144	18600
4	0.00	0.00	145	18700
5	0.00	0.00	148	18200
6	0.00	0.00	142	18600
Mean	0.00	0.00	146	18600
CV (%)[e)]	NA[f)]	NA	2.63	1.41

a) Rat plasma, containing no analyte or IS, were extracted and analyzed.

b) Rat plasma, containing only IS, were extracted and analyzed.

c) LLOQ: lower limit of quantification.

d) HQC: high quality control.

e) CV (%) = standard deviation / mean × 100.

f) NA: not applicable.

Table 2. Calibration curves generated for LB in rat plasma.

Batch	**Slope**	**Intercept**	***R***
1	0.166	2.98	1.00
2	0.174	1.39	0.999
3	0.153	3.78	0.999
Mean	0.164	2.72	0.999
CV (%)[a)]	6.45	NA[b)]	NA

a) CV (%) = standard deviation / mean × 100.

b) NA: not applicable.

3.1.5. Matrix Effect and Recovery

The matrix effect and recovery was estimated in six different rat plasma samples by comparing the mean area of the analyte peaks from extracted QC samples at concentrations of 150, 1000, and 8000 ng/mL. The absolute matrix effect was ranged from 112 to 135% and from 87.2 to 88.1% for LB and rosiglitazone, respectively (Table 4). The relative matrix effect was assessed based on the direct comparison of the peak areas of LB and rosiglitazone added to post-extraction samples of plasma from six different sources of rat plasma (set 2). The precision of determination of set 2 (i.e., relative matrix effect) ranged from 1.60 to 3.59% for LB and from 2.89 to 4.51% for rosiglitazone. The variability appeared comparable to the variability data obtained using the standard solution in which the analyte was dissolved in acetonitrile (set 1; LB: 2.26-5.65%, rosiglitazone: 2.10-7.94%); these data confirmed the absence of the relative matrix effects for LB and rosiglitazone. The precision values (CV) of the LB/rosiglitazone ratio was ranged from 5.79-7.92% for the samples that were spiked into blank extracts post-extraction and from 2.15-7.04% for the standards injected directly in acetonitrile. These findings indicate that the absolute and relative matrix effects for the LB/rosiglitazone ratios of the peak areas were insignificant to determination LB levels following its addition to six different lots of rat plasma.

The overall recovery of LB was 79.0, 93.3 and 97.8% for 150, 1000 and 8000 ng/mL concentration levels, respectively and the recovery for rosiglitazone (i.e., the IS) was found to be 77.2, 90.0 and 86.8% (Table 4). Collectively, these observations indicate that the current sample processing conditions support adequate recoveries for both the analyte and the IS.

3.1.6. Stability

The stability of the analyte were also examined under the various conditions used in the handling and storage of the standards and samples (Tables 5 and 6). The stability of the LB stock solution (250 ng/mL) was assessed over a 6 h period at room temperature (20°C) and over a 3 week period under refrigeration (4°C); six replicates were assessed under each condition. Relative to the LB concentration in a fresh sample (indicated as 0 h in Table 5), the LB concentrations of the samples stored in 20°C and 4°C were 99.2% and 99.6% (Table 5), respectively.

After standing at room temperature for 24 h (indicated as bench-top stability in Table 6), the QC samples of LB (150 ng/mL and 8000 ng/mL) had concentrations of –2.82% and –0.557%, respectively, which were close to the theoretical value. Similarly, a post-preparative stability assessment indicated that the LB concentrations in the 150 and 8000 ng/mL samples differed by –1.38 and –0.935%, respectively, from the theoretical values for these concentrations. Three cycles of freeze-thaw had no effect on the stability of

LB as evidenced by the fact that the estimated concentration was only slightly different from the theoretical values (i.e., –5.71% for 150 ng/mL and 1.34% for 8000 ng/mL in Table 6).

Furthermore, after storage at –80°C for long-term stability, the estimated concentrations of the 150 and 8000 ng/mL samples –2.18% and 1.49%, respectively (Table 6). These were close to the real values and demonstrate that the long-term storage of rat plasma samples at –80°C was adequate for the maintenance of LB stability. Thus, handling, processing, and storage conditions used in the present study maintained the stability of the LB concentrations in the rat plasma samples and did not affect the estimation of the LB concentrations.

Table 3. Summary of quality control samples for LB in rat plasma.

Batch	Theoretical concentration (ng/mL)				
	LLOQ[a)]	**LQC[b)]**	**MQC[c)]**	**HQC[d)]**	**Diluted HQC[e)]**
	50	**150**	**1000**	**8000**	**8000**
(A) Intra-day accuracy and precision					
Number of samples	6	6	6	6	6
Mean concentration	46.4	143	1060	7550	7920
CV (%)[f)]	1.31	5.74	2.34	3.60	1.88
RE (%)[g)]	–7.20	–4.38	5.65	–5.63	–0.957
(B) Inter-day accuracy and precision					
Number of samples	18	18	18	18	
Mean concentration	47.3	144	1020	7750	
CV (%)	5.05	5.04	4.33	3.97	
RE (%)	–5.33	–4.00	1.70	–3.18	

a) LLOQ: lower limit of quantification.

b) LQC: low quality control.

c) MQC: middle quality control.

d) HQC: high quality control.

e) Diluted HQC = QC samples were analyzed after a tenfold dilution with blank rat plasma (i.e., 80000 → 8000 ng/mL).

f) CV (%) = standard deviation of the concentration / mean concentration × 100.

g) RE (%) = (calculated concentration – theoretical concentration) / theoretical concentration × 100.

Table 4. Matrix effect, recovery, and precision (CV, %) for LB and rosiglitazone (internal standard) in six different lots of rat plasma.

Nominal concentration (ng/mL)	Absolute matrix		Recovery[b] (%)		Precision[c] (CV, %)					
					LB		IS		LB/IS	
	LB	IS	LB	IS	Set 1	Set 2	Set 1	Set 2	Set 1	Set 2
150	135	87.2	79.0	77.2	5.65	3.02	4.15	2.89	7.04	5.79
1000	124	87.4	93.3	90.0	2.26	1.60	2.10	4.51	2.15	5.84
8000	112	88.1	97.8	86.8	5.13	3.59	7.94	3.80	5.38	7.92

a) Absolute matrix effect expressed as the ratio of the mean peak area of an analyte added post-extraction (set 2) to the mean peak area of the same analyte standards (set 1) multiplied by 100.

b) Recovery calculated as the ratio of the mean peak area of an analyte added before extraction to the mean peak area of an analyte spiked post-extraction (set 2) multiplied by 100.

c) Precision of determination of peak areas of LB and rosiglitazone, and peak area ratios (LB/rosiglitazone) in set 1 and 2 as the measure of relative matrix effect.

Table 5. Stability of LB in stock solutions.

Batch	Stability[a] (peak area)		
	0 h (initiation)	**6 h (room temp.)**	**3 weeks (refrigerated)[b]**
Number of samples	6	6	6
Mean response	1860	1840	1850
CV (%)[c]	1.29	0.722	1.44
Relative concentration (%)[d]	100	99.2	99.6

a) Stock solutions were diluted to 250 ng/mL for analysis.

b) Stock solutions were stored at 4°C.

c) CV (%) = standard deviation of the concentration / mean concentration × 100.

d) Relative concentration (%) = the measured value / the initial value.

Table 6. Stability of quality control samples.

Batch	Theoretical concentration (ng/mL)	
	150	**8000**
(A) Bench-top stability at room temperature for 24 h		
Number of samples	3	3
Mean concentration	146	7960
CV (%)[a)]	2.04	2.14
RE (%)[b)]	–2.82	–0.557
(B) Post-preparative stability at 4°C for 3 days		
Number of samples	3	3
Mean concentration	148	7930
CV (%)	4.72	2.28
RE (%)	–1.38	–0.935
(C) Freeze-thaw stability (3 cycles)		
Number of samples	3	3
Mean concentration	141	8110
CV (%)	1.69	0.799
RE (%)	–5.71	1.34
(D) Long-term stability* for *2 weeks		
Number of samples	3	3
Mean concentration	147	8120
CV (%)	2.19	2.66
RE (%)	–2.18	1.49

a) CV (%) = standard deviation of the concentration / mean concentration × 100.

b) RE (%) = (calculated concentration – theoretical concentration) / theoretical concentration × 100.

3.1.7. Applicability for Use in Pharmacokinetic Studies

To assess the applicability of the present assay for use in pharmacokinetic studies, the assay was used to determine the plasma concentrations of LB in female rats that had received an oral dose of LB (1 mg/kg). The temporal profile of the mean LB plasma concentrations is shown in Fig. 3. The concentrations of LB were readily measurable for all plasma samples that were collected within 24 h of administration, which suggests that the current assay adequately determined the pharmacokinetic characteristics of LB following an oral dose. The calculated pharmacokinetic parameters, including C_{max}, T_{max}, $t_{1/2}$, MRT_{inf}, and AUC_{inf}, were listed in Table 7.

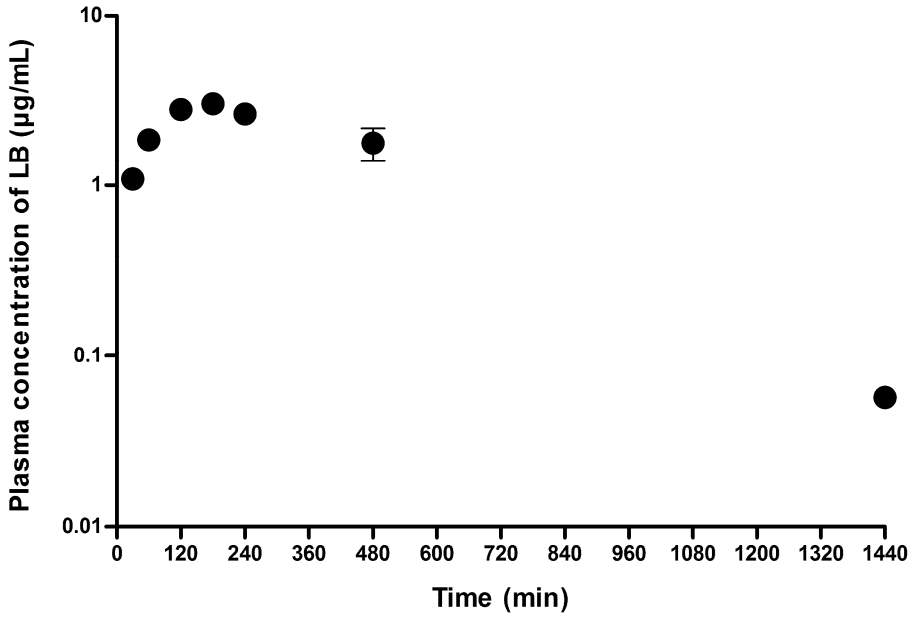

Figure 3. Temporal profile of plasma concentration of LB in female rats receiving an oral administration of 1 mg/kg LB. Data are expressed as the mean ± S.D. of triplicate runs.

Table 7. Pharmacokinetic parameters of LB following an oral administration of LB at a dose of 1 mg/kg in female rats. Data are expressed as the mean ± S.D. of triplicate runs.

Parameters	**1 mg/kg**
AUC_{inf} (μg · min/mL)	2040 ± 524
C_{max} (μg/mL)	3.05 ± 0.160
T_{max} (min)	140 ± 34.6
$t_{1/2}$ (min)	317 ± 157
MRT_{inf} (min)	522 ± 220

3.2. *In vitro* Absorption, Distribution and Elimination Studies

3.2.1. PAMPA

Similar to previous studies that reported estimated P_{app} values of ~7.4×10^{-6} cm/sec (Kerns et al., 2004; Zhu et al., 2002), the estimated P_{app} value for verapamil in the present study was $8.66 \pm 0.0978 \times 10^{-6}$ cm/sec. This finding indicates that the current assay adequately estimated membrane permeability. The estimated value for P_{app} of LB was approximately $1.19 \pm 0.142 \times 10^{-6}$ cm/sec, the value corresponding to the predicted human bioavailability of 72.1%. Additionally, LB sulfate, a soluble salt form of the activator, had an estimated P_{app} value of $7.39 \pm 0.0174 \times 10^{-6}$ cm/sec which suggests that the permeability of LB across the artificial membrane is high. The recoveries of LB and verapamil were almost complete (>92%).

3.2.2. Permeability Study with MDCKII Cells

In the present study, intestinal permeability was estimated using MDCKII cell monolayers. Previous reports have demonstrated that the permeability of various compounds across an epithelial cell monolayer is significantly correlated with bioavailability in humans (Feng et al., 2008). In the present study, the transport of LB (5 μM) was determined at 2 h in both the apical-to-basolateral (A to B) and basolateral-to-apical (B to A) directions in wild type MDCKII cell monolayers (Table 8). The A to B transport was estimated to be $0.533 \pm 0.0914 \times 10^{-6}$ cm/sec whereas the B to A transport was estimated to

be 5.02 ± 0.510 × 10^{-6} cm/sec. The P_{app} value for A to B transport, which is the value relevant for the intestinal absorption, indicated that bioavailability in humans is approximately 43.2% (Irvine et al., 1999). To determine whether MDR1 is involved in the limited transport of LB in the absorptive direction, a similar bidirectional transport study was carried out investigating the transport of LB in MDCKII-MDR1 cell monolayers (Table 8). Although the A to B permeability was relatively unchanged (i.e., from 0.533 to 0.433 × 10^{-6} cm/sec, Table 8), the B to A transport value was significantly increased in MDR1 cells (i.e., from 5.02 to 8.28 × 10^{-6} cm/sec, $p<0.05$).

To further examine the involvement of MDR1 mediated LB efflux in MDCKII cells, a bidirectional transport study was carried out for 5 μM LB in the presence of 500 μM verapamil (i.e., an inhibitor for MDR1) in wild type MDCKII cells as well as MDCKII-MDR1 cells (Table 8). The addition of verapamil was associated with a significant increase in A to B transport (i.e., from 0.533 to 4.14 × 10^{-6} cm/sec for wild type cells, $p<0.001$; from 0.433 to 4.06 × 10^{-6} cm/sec for MDR1 cells, $p<0.001$) while the extent of change for B to A transport was much less (Table 8). As a result, the efflux ratio was reduced (i.e., from 9.42 to 1.33 for wild type cells; from 19.1 to 1.72 for MDR1 cells) as the addition of verapamil. These observations indicate that LB is transported via the MDR1 efflux transporter.

Table 8. Apparent permeability coefficients and efflux ratios for LB across MDCKII-MDR1 cell monolayers in the absence and the presence of verapamil (500 μM). Data are expressed as the mean ± S.D. of quadruplicate runs.

LB (5 μM)	**P_{app} (× 10^{-6} cm/sec)**		**Efflux ratio**
	A to B	**B to A**	
Wild Type	0.533 ± 0.0914	5.02 ± 0.510	9.42
MDR I	0.433 ± 0.123	8.28 ± 1.76	19.1
Wild Type + Verapamil	4.14 ± 0.691	5.52 ± 0.769	1.33
MDR I + Verapamil	4.06 ± 0.618	6.98 ± 0.418	1.72

3.2.3. Interaction of LB with SLC, MDR1 and BCRP Transporters

In this study, also investigated whether LB would interact with six major transporters selected based on a regulatory recommendation from the United States Food and Drug Administration (Prueksaritanont et al., 2013). The cellular accumulations of the representative substrates were assessed in the presence of varying concentrations of LB and the percent transport activity was plotted against the substrate concentration (Fig. 4). Next, the IC_{50} was estimated. In general, the inhibitory potential of LB was very weak for SLC transporters such as OATP1B3, OAT1 and OCT2, while the interaction was readily measured for OATP1B1 and OAT3 (Fig. 4). The estimated IC_{50} values were 2.44 ± 1.23 μM, 216 ± 187 μM, 151 ± 36.9 μM and 34.3 ± 33.9 μM for OATP1B1, OATP1B3, OAT1 and OAT3, respectively. The plasma concentrations observed in these pharmacokinetic studies were consistently less than 20 μM, which is the initial plasma concentration following a 2 mg/kg IV injection (see Section 3.3). This suggests that the inhibition of SLC transporters, except for OATP1B1, by LB was less likely.

For MDR1, IC_{50} was estimated based on the inhibition of digoxin efflux by LB (Fig. 5). In this study, a higher cellular accumulation would be regarded as the inhibition of digoxin efflux. LB concentration dependency was readily evident with the estimated IC_{50} of 12.5 ± 3.61 μM. For the case of BCRP, a

bidirectional transport study was carried out for methotrexate (i.e., standard substrate for the transporter) in the absence and presence of LB (i.e., 200 μM, final concentration) in MDCKII-BCRP cell monolayers. The addition of LB affected the transport to a certain extent (i.e., for A to B transport, 0.508 ± 0.0490 × 10^{-6} cm/sec 'without LB', 1.27 ± 0.205 × 10^{-6} cm/sec 'with LB'; for B to A transport, 1.93 ± 0.0803 × 10^{-6} cm/sec 'without LB', 3.18 ± 0.121 × 10^{-6} cm/sec 'with LB'). As a result, the efflux ratio did not appear to change (i.e., from 3.79 for 'without LB' to 2.49 for 'with LB'). These observations indicate that the involvement of BCRP in the transport of LB is weak.

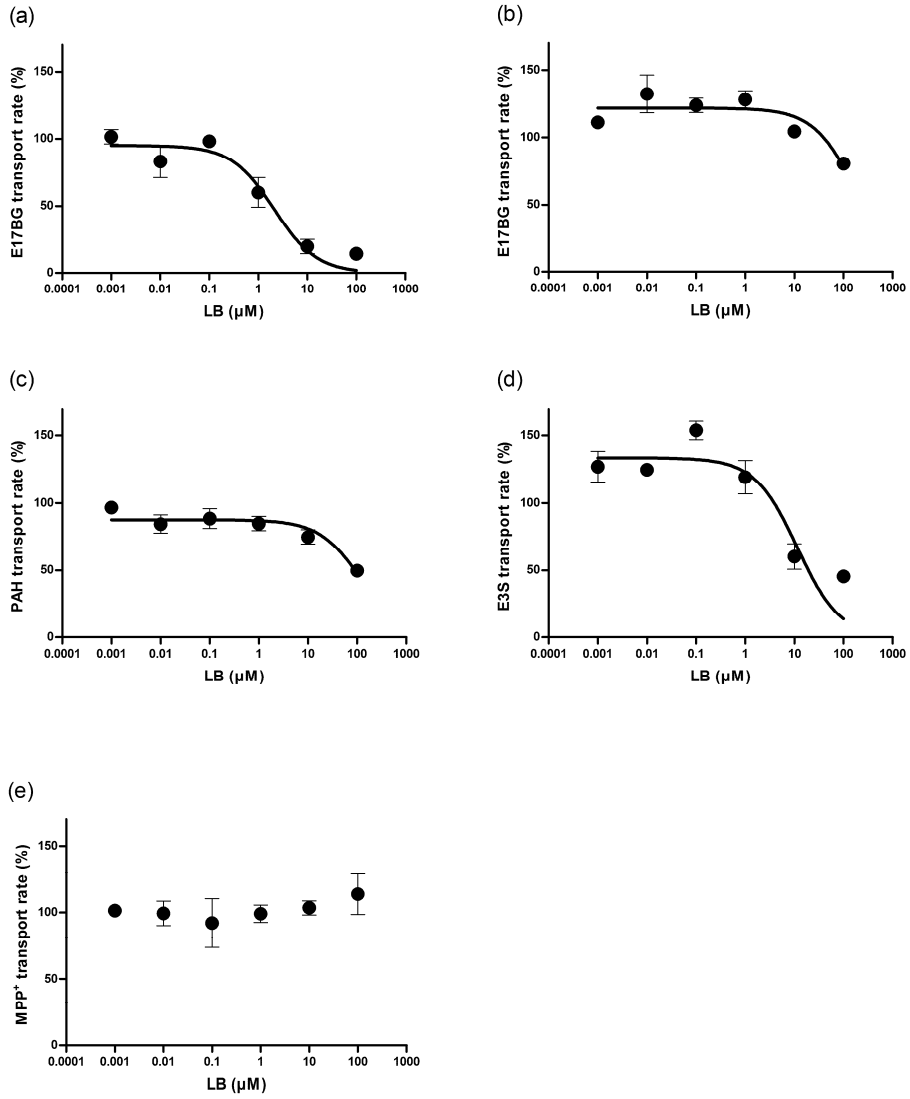

Figure 4. Inhibitory effects of LB on the uptake of (a) estradiol-17β-glucuronide (E17BG) into MDCK-OATP1B1, (b) E17BG into MDCK-OATP1B3, (c) p-aminohippuric acid (PAH) into MDCK-OAT1, (d) estrone-3-sulfate (E3S) into MDCK-OAT3, and (e) 1-methyl-4-phenylpyridinium (MPP^+) into MDCK-OCT2 cells. Data are expressed as the mean ± S.D. of triplicate runs.

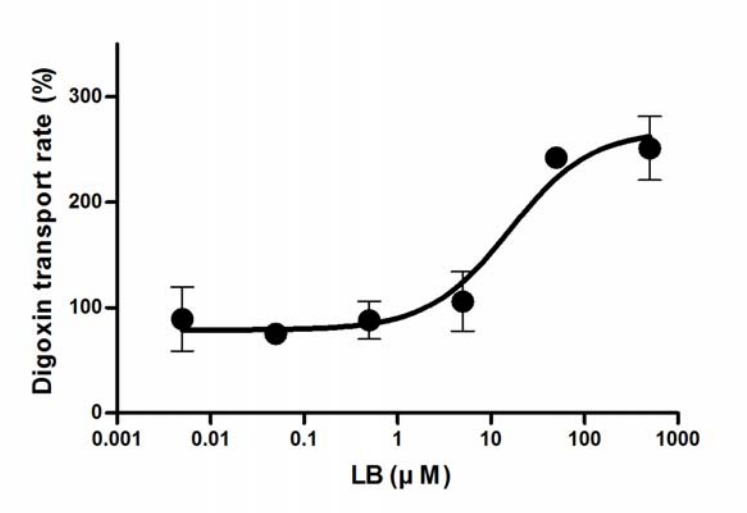

Figure 5. Effects of inhibitors of LB on the cellular accumulation of digoxin in MDCK-Flip-in-MDR1 cells grown on solid supports. Data are expressed as the mean ± S.D. of triplicate runs.

3.2.4. Standard PCR-based Cloning Strategy and the Interaction of LB with SLC, MDR1 and BCRP Transporters

The possibility of LB interacting with six major transporters was examined. The following standard PCR-based cloning strategy [i.e., amplification of the target (i.e., transporter) region according to polymerase chain reaction, ligation into vector and transformation] was employed to obtain functional clones.

3.2.4.1. Amplification Conditions

3.2.4.1.1. OATP1B1

cDNA was obtained by RNA LA PCR kit (Takara, Shiga, Japan) from human liver total RNA (Clontech, Palo Alto, CA, USA) under the following conditions: 42°C for 30 min, heating to 99°C for 5 min, and subsequently cooling to 4°C. PCR amplification was performed in 30 cycles using Ex Taq DNA polymerase (Takara) under the following conditions: denaturation at 95°C for 1 min, annealing at 58°C for 1 min, and elongation at 72°C for 2 min.

3.2.4.1.2. OATP1B3

cDNA was obtained by RNA LA PCR kit (Takara) from human liver total RNA (Clontech) under the following conditions: 42°C for 30 min, heating to

99°C for 5 min, and subsequently cooling to 4°C. PCR amplification was performed in 30 cycles using PrimeStar HS DNA polymerase (Takara) under the following conditions: denaturation at 98°C for 10 sec, annealing at 60°C for 5 sec, and elongation at 72°C for 2.2 min.

3.2.4.1.3. OAT1

cDNA was obtained by RNA LA PCR kit (Takara) from human liver total RNA (Clontech) under the following conditions: 42°C for 30 min, heating to 99°C for 5 min, and subsequently cooling to 4°C. PCR amplification was performed in 30 cycles using PrimeStar HS DNA polymerase (Takara) under the following conditions: denaturation at 98°C for 10 sec, annealing at 60°C for 5 sec, and elongation at 72°C for 2.2 min.

3.2.4.1.4. OAT3

cDNA was obtained by Maxim PreMix (Intron Bio, Seongnam, Korea) from human kidney total RNA (Clontech) under the following conditions: 42°C for 60 min, heating to 95°C for 5 min, and subsequently cooling to 4°C. PCR amplification was performed in 30 cycles using Ex Taq DNA polymerase (Takara) under the following conditions: denaturation at 94°C for 30 sec, annealing at 59°C for 30 sec, and elongation at 72°C for 2 min.

3.2.4.1.5. OCT2

cDNA was obtained by PrimeScript 1st strand cDNA synthesis kit (Takara) from human kidney total RNA (Clontech) under the following conditions: 42°C for 60 min, heating to 95°C for 5 min, and subsequently cooling to 4°C. PCR amplification was performed in 30 cycles using Ex Taq DNA polymerase (Takara) under the following conditions: denaturation at 94°C for 30 sec, annealing at 65°C for 30 sec, elongation at 72°C for 100 sec.

3.2.4.1.6. MDR1

The entire ORF sequence of human MDR1 was amplified from cDNA prepared from the human liver tissue (Biochain, Hayward, CA, USA). The PCR product was initially cloned into the pEF6/V5-His TOPO® TA plasmid (Invitrogen) and analyzed by direct sequencing. The sequenced clone was found to harbor naturally occurring genetic variations at the cDNA positions at 2677 and 3435. Thus the site-directed mutagenesis (Stratagene, La Jolla, CA, USA) was carried out to obtain the human MDR1 sequence and the final product was verified by direct sequencing.

3.2.4.2. Ligation

The PCR primers are synthesized by Bioneer (Daejeon, Korea) and the specific sequences are listed in Table 9. The amplicon for OATP1B1, OATP1B3 or OAT3 was directly digested with Kpn I / Not I (OATP1B1), Kpn

I / Xho I (OATP1B3) or Hind III / Xho I (OAT3) and cloned into pcDNA5/ FRT vector (Invitrogen). OAT1 and OCT2 amplicons were cloned into pCRII vector (Invitrogen) and subsequently subcloned into pcDNA5/FRT. For the case of MDR1, the sequence was subcloned into pcDNA5/FRT vector (Invitrogen) using Bam HI / Not I restriction enzyme. Any insertion or deletion of the gene of interest was confirmed by sequencing, and site-directed mutagenesis (Stratagene) carried out if necessary.

3.2.4.3. Transfection

The pcDNA5/FRT vectors containing each ORF sequence were transfected using Fugene HD transfection reagent (Promega, Madison, WI, USA) into MDCK cells modified by Flp-In system (Invitrogen, Carlsbad, CA) (Kim et al., 2010). Subsequently, the transfected cell was cultured and selected by culture media containing 100 μg/mL of hygromycin (Invitrogen) for 3 weeks.

3.2.4.4. Biochemical Confirmation of Transporter Gene Expression

RT-PCR analyses were performed to identify the expression of transport systems in MDCK cells. Total mRNA was extracted from MDCK cells using an RNeasy Mini Kit (Qiagen, Valencia, CA, USA) according to the manufacturer's instructions. After isolation, the concentration and purity of the extracted RNA were confirmed by UV spectrophotometry at 260/280 nm. Reverse transcription was carried out under the following conditions using an

Maxime RT PreMix (Intron Bio): 42°C for 60 min, heating to 99°C for 5 min and subsequently cooling to 4°C. The specific primers used in the PCR reactions are provided in Table 10. Ex Taq DNA polymerase (Takara) was used to conduct PCR amplification and the thermocycling conditions were as follows: denaturation at 98°C for 10 sec, annealing at 55°C for 30 sec, elongation at 72°C for 30 sec, 30 cycle. The PCR products were separated by gel electrophoresis on 1% (w/v) agarose, inspected under UV light after ethidium bromide staining, and photographed with a digital camera (Fig. 6).

3.2.4.5. Functional Confirmation of Transporter Expression

Functional activity for MDCK-OATP1B1, MDCK-OATP1B3, MDCK-OAT1, MDCK-OAT3, MDCK-OCT2, and MDCK-Flp-in-MDR1 was confirmed by comparing cellular accumulation of substrates [i.e., [^{3}H] p-aminohippuric acid (OAT1) (Aslamkhan et al., 2003), [^{3}H] estrone-3-sulfate (OAT3) (Brandoni et al., 2006), [^{3}H] estradiol-17β-glucuronide [OATP1B (Izumi et al., 2013; Matsushima et al., 2005) and OATP1B3 (Brandoni et al., 2006)], [^{3}H] 1-methyl-4-phenylpyridinium (OCT2) (Umehara et al., 2008), and [^{3}H] digoxin (MDR1) (Kurihara et al., 1988; Schinkel et al., 1997; Song et al., 1999)] between the mock cells and cells expressing the corresponding transporter. In addition, it was further confirmed the functional expression by examining the significant depression of the functional activity by the addition of standard inhibitor of the transporter [i.e., rifampin for OATP1B1 (Treiber

et al., 2007) and OATP1B3 (Kindla et al., 2011; Treiber et al., 2007); probenecid for OAT1 (Uwai et al., 1998); rosuvastatin for OAT3 (Windass et al., 2007); quinine for OCT2 (Fujita et al., 2006); verapamil for MDR1 (Muller et al., 1995)] were seeded at a density of 5×10^5 cells/well in 24-well plates (Fig. 7). After 2 days, cells are washed twice and pre-incubated with the buffer medium of Hank's balanced salts solution (HBSS), 25 mM HEPES, and 25 mM glucose (pH 7.4). Cells are incubated for 10 min in 37°C with the buffer medium containing 1 μM radiolabeled substrates in the absence and presence of the inhibitor (1 mM). After 10 min of incubation, the medium was removed, and cells were then washed three times with ice-cold Dulbecco's phosphate-buffered saline (DPBS), followed by solubilization in 0.2 N NaOH. The amount of substrate accumulated within the cell was determined by liquid scintillation counter (Tri-Carb 3110 TR, Perkin-Elmer Life Science), and normalized relative to the cell lysate protein concentration, as determined by BCA assay.

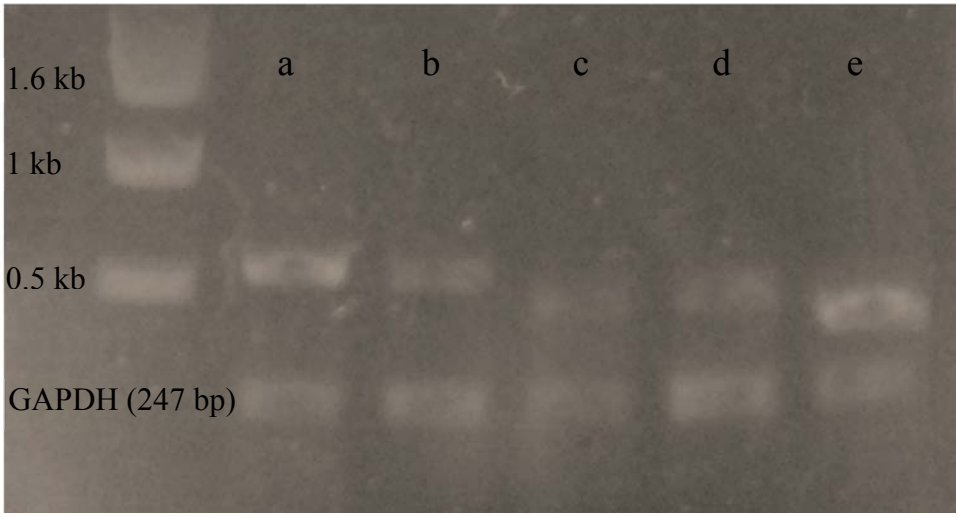

Figure 6. Agarose gel electrophoresis of RT-PCR product using the primers listed in Table 10 with the total RNA extract from MDCK cell line expressing the corresponding transporter. Key: Lane a, OATP1B1 expressing MDCK cells; Lane b, OATP1B3 expressing MDCK cells; Lane c, OAT1 expressing MDCK cells; Lane d, OAT3 expressing MDCK cells; Lane e, OCT2 expressing MDCK cells. The numbers in the most left lane represents the expected molecular size of the band. The term 'GAPDH (247 bp)' represents the location of the amplified housekeeping gene having the molecular size of 247 bp.

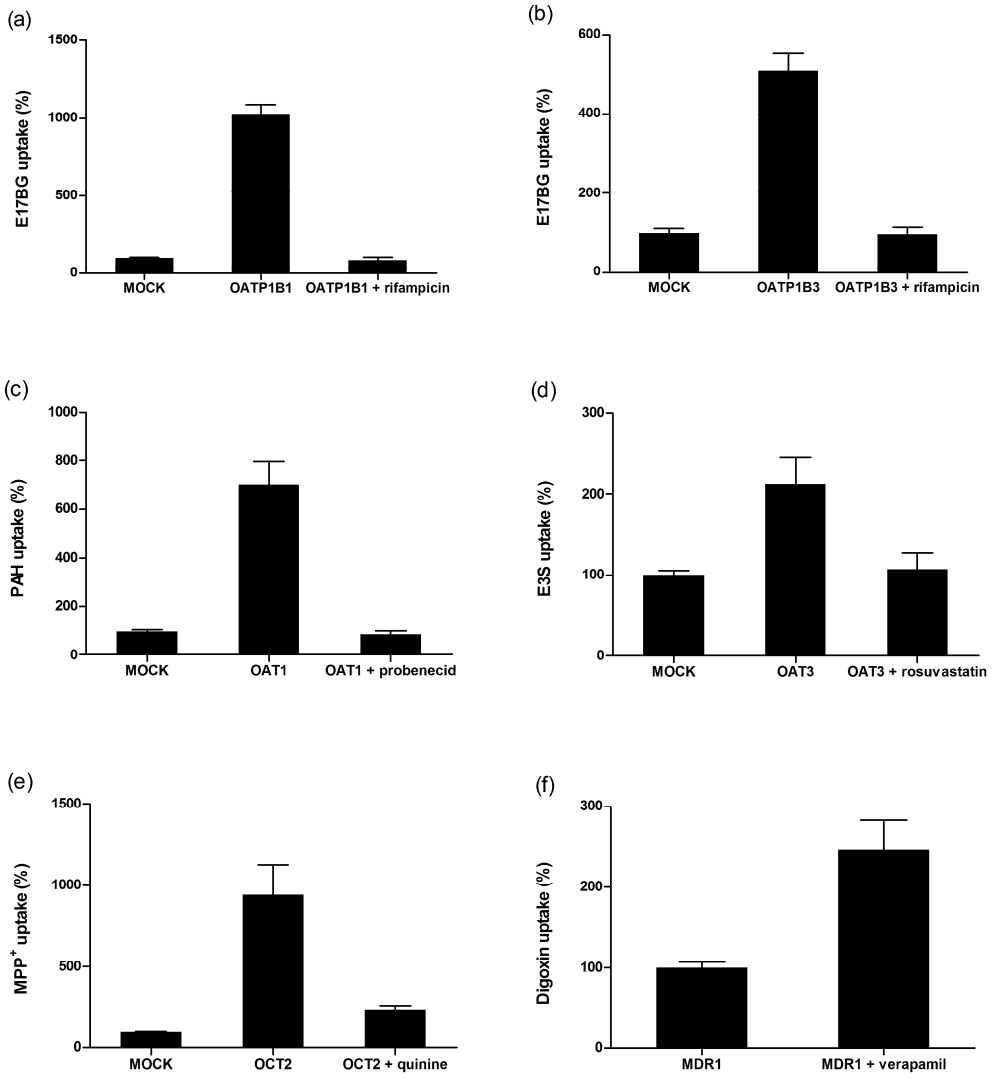

Figure 7. Relative transport rate for MDCK cells expressing SLC transporters (a-e) and MDR1 (f). Key: Bars indicated as 'MOCK' represents the relative uptake rate (in percent of control) in mock cells (i.e., empty vector transfected cell), bars indicated as each transporter pathway represents the uptake rate in MDCK cells expressing the corresponding transporter, and bars indicated

with the transport pathway + inhibitors represents the uptake rate in MDCK cells expressing the corresponding transporter in the presence of the known inhibitor. In panels a and b. estradiol-17β-glucuronide (E17BG) 1 μM as substrate, rifampicin 1 mM as inhibitor; in panel c. p-aminohippuric acid (PAH) 1 μM as substrate, probenecid 1 mM as inhibitor; in panel d. estrone-3-sulfate (E3S) 1 μM as substrate, rosuvastatin 1 mM as inhibitor; in panel e. 1-methyl-4-phenylpyridinium (MPP+) 1 μM as substrate, quinine 1 mM as inhibitor; in panel f. digoxin 1 μM as substrate, verapamil 500 μM as inhibitor. Data are expressed as the mean ± S.D of triplicate runs.

Table 9. List of cloning primer sequences.

Transporter		Cloning primer sequence
OATP1B1	forward	5’-CCCGGTACCGCCGCCACCCAGGTGATTGTTTCAAACTG-3’
	reverse	5’-CCGGCGGCCGCTCTAGAGCAATGCTGTTTGGAAACAC-3'
OATP1B3	forward	5’-CCCGCGGCCGCGCCGCCACCCAAACCAAGCATCAGCAACA-3’
	reverse	5’-CCGCTCGAGTGCAATGTTAGTTGGCAGCA-3’
OAT1	forward	5‘-CAACCCAGCTGCGGAGGCAA-3’
	reverse	5‘-AGGGAGGTGGACCCCTGGGA-3’
OAT3	forward	5'-CCCAAGCTTGCCGCCACCATGACCTTCTCGGAGATCCTG-3‘
	reverse	5'-CCGTCTAGATCCACCAGTCTTCAGCGGGAT-3‘
OCT2	forward	5'-CGCTTAATCCAAGGACTGGT-3'
	reverse	5'-ATCACAATGGCCTATGAGAT-3'

Table 10. List of primer sequences for the confirmation of transporter gene expression.

Transporter		primer sequence	product size (bp)
OATP1B1	forward	5'-GAATTGCCAAATTCTCATG-3'	600
	reverse	5'-GTTGGTGGACCACTTTATA-3'	
OATP1B3	forward	5'-TCGTGGCATAGGGGAAACCC-3'	550
	reverse	5'-GACTGACCGTACTGTTGCTC-3'	
OAT1	forward	5'-TGAATGTGGAGTGGATGCCC-3'	477
	reverse	5'-AGATGCTGACTCCAAAGCCC-3'	
OAT3	forward	5'-CGCAAGTGACCTGTTCCGG-3'	500
	reverse	5'-CCCGTAGATGATATTGGGG-3'	
OCT2	forward	5'-GCTACGAGGTGGACTGGAAC-3'	433
	reverse	5'-CTCCGATATCTCCGCCCAAC-3'	
GAPDH	forward	5'-AACATCATCCCTGCTTCCAC-3	247
	reverse	5'-GACCACCTGGTCCTCAGTGT-3	

3.2.5. Plasma Protein Binding and Blood-Plasma Partitioning of LB

In this study, the extent of LB binding to rat plasma proteins was examined using an ultrafiltration method. In the rat plasma, the unbound fractions of LB at concentrations of 0.1, 0.5, and 2.5 μg/mL were 0.352 ± 0.194%, 0.201 ± 0.0111% and 0.147 ± 0.0426% respectively, suggesting that LB binds extensively to rat plasma proteins. The percent of unbound LB was also determined by RED. The findings indicated that plasma protein binding, as measured by the dialysis method, was also extensive (0.549 ± 0.0759%, at a final LB concentration of 2.5 μg/mL) and was not affected by the LB concentration. The blood/plasma concentration ratios of LB at 0.1 and 2.5 μg/mL were 139 ± 13.0% and 126 ± 13.8%, respectively. This indicates that there is no appreciable distribution of LB to blood cells and that the concentrations of LB in the plasma and blood are almost identical.

3.2.6. Metabolic Stability of Liver Microsomes

The assessment of the metabolic stability of LB required that it be independently incubated for 30 min with rat liver microsomes in the presence of either NADPH or UDPGA. The LB level in rat liver microsomes significantly decreased to approximately 56% of its initial concentration after being incubated with NADPH (Fig. 8a). Under similar conditions in rat liver microsomes, the concentration of testosterone, a positive control, decreased

with a half-life of 2.1 ± 0.1 min, while the concentration of LB remained relatively unchanged after 30 min of incubation in the presence of UDPGA (Fig. 8b). However, 7-hydroxycoumarin (7-OH), a positive control for glucuronidation, disappeared completely within 5 min of the start of the reaction. This suggests that the microsomal fractions contained an adequate level of glucuronidation activity.

(a)

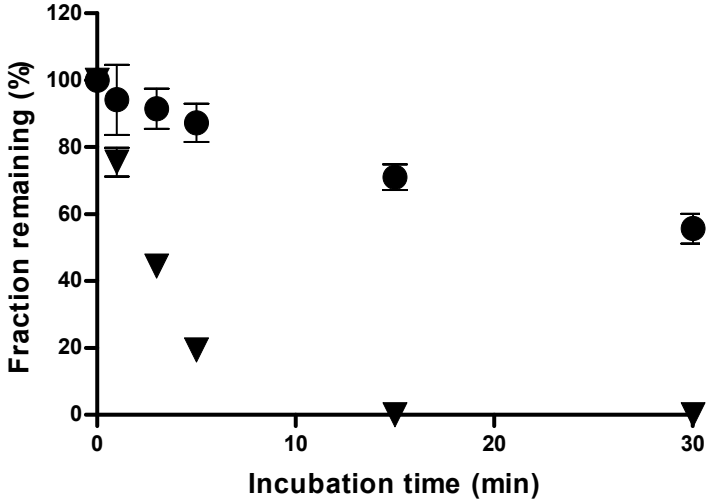

(b)

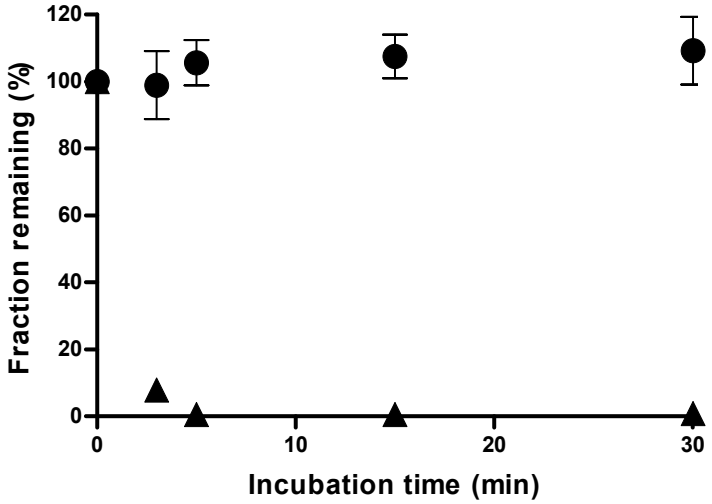

Figure 8. Metabolic stability profiles of LB in pooled rat liver microsomes. Rat liver microsomes were incubated with LB (10 μM) for 30 min in the presence of (a) NADPH or (b) UDP-glucuronic acid as a cofactor. Symbols: LB (●), testosterone (▼) and 7-hydroxycoumarine (▲). Data are expressed as the means ± S.D. of triplicate runs.

3.2.7. Inhibition of Cytochrome P450

To determine where LB would influence the generation of CYP-specific metabolites in humans, the inhibition of CYP was investigated by incubating CYP isozymes in the presence of NADPH and typical CYP substrates [viz, 1A2 (phenacetin), 2C9 (tolbutamide), 2C19 (s-mephenytoin), 2D6 (dextromethorphan) and 3A4 (nifedipine or testosterone)]. In the presence of LB, the metabolism of CYP 1A2, 2C9, and 2C19 were inhibited by 41.0 ± 6.56%, 50.1 ± 5.71% and 43.2 ± 3.71%, respectively (Table 11). When incubated with substrates from other pathways, the degree of reduction was less than 20% (viz, 4.90 ± 3.60% for 2D6, 16.1 ± 5.48% using nifedipine for 3A4, and 31.0 ± 13.1% using testosterone for 3A4), suggesting that these pathways play a minor role in inhibiting the CYP enzyme activity of LB (Table 11).

Table 11. Percent inhibition on metabolism of substrate incubated with 10 μM LB in human liver microsomes. Data are expressed as the mean ± S.D. of triplicate runs.

CYP isozymes	Inhibition (%)
CYP1A2 (phenacetin)	41.0 ± 6.56
CYP2C9 (tolbutamide)	50.1 ± 5.71
CYP2C19 (s-mephenytoin)	43.2 ± 3.71
CYP2D6 (dextromethorphan)	4.90 ± 3.60
CYP3A4 (nifedipine)	16.1 ± 5.48
CYP3A4 (testosterone)	31.0 ± 13.1

3.2.8. Metabolite Identification of LB in Rat Liver Microsomes

The biotransformation of the metabolite is confirmed by comparing the spectrum of the metabolite to that of the parent. Further identification of the transformation location can be assessed upon the availability of the structure of the parent. The instrumental response for the MRM transition of the parent or any targeted metabolites in Table 12 was equally selected by the IDA criteria. Since the metabolite standards are usually not available in early drug discovery, instrumental performance on the parent transition can present a good estimation for the detection of most structurally similar metabolites for this method.

The extracted ion chromatograms of parent and its five metabolites (Fig. 9), and EPI spectra of LB, demethylated LB and hydroxylated LB were from one single injection of 100 μM LB incubated in rat liver microsome for 30 min. Single chromatographic peaks of parent and metabolites were extracted from the total ion chromatogram.

During the study of LB metabolic stability, assignment of the detected masses as metabolites (Fig. 10) was based on the following criteria: (1) the EMS and MRM signal should be detected in the sample incubated with RLM (time 30 min), but undetectable in the 0-min control sample, (2) an expected mass of the metabolite ion should be observed from EPI spectra, (3) either the same product ions or equivalent neutral losses were found from the EPI

spectra of LB and its metabolites. Metabolism pathways of LB were proposed based on the mass shift of the metabolites, fragmentation pattern obtained from EPI spectra, as well as the intensity of the MRM signal (Fig. 9 and Fig. 10).

The metabolites (M1 and M2) identified as the product of demethylation of 4-methoxyphenoxy group (M1) and N-demethylation (M2) showed major portion of metabolites were proposed as demethylated LB (Fig. 10 and Table 13) because the precursor ion (m/z 467.3) and/or the product ions (m/z 244.2 and/or m/z 138.1) were 14 mass units smaller than the corresponding precursor (m/z 481.2) and product ions (m/z 258.1 or m/z 152.2) of LB.

The fragmentation pattern of M1 is quite similar to LB. These findings suggested that demethylation took place at the part of the molecule corresponding to the m/z 152.2 (Fig. 9 and Table 13). M1 and M2 were likely to be both fragmentation products produced from LB at m/z 244.2 to yield closely spaced peaks. However, these two peaks were distinctly different in that m/z values for M1 and M2 were 152.2 and 138.1, respectively. For the case of other metabolites, the metabolites M3 and M4 appeared to be formed by hydroxylation [i.e., M+H+17; i.e., m/z 497.2→274.2, 497.2→258.2, and 497.2→152.1], while M5 may be a di-demethylated form of LB (M+H–28),

with m/z 453.2→230.2. The overall metabolic pathway in vitro was proposed for LB in rats based on these observations, as shown in Fig. 11.

The intensity of the mono-demethylated LB (i.e., M1) appeared to be the highest (Fig. 9), suggesting that this metabolite is the major species that is produced under in vitro conditions. In fact, the signal intensity for M1 was approximately two-fold higher than that of M2; For the case of the other metabolites, the intensities were even lower (Fig. 9) than that of M2.

(a) TIC

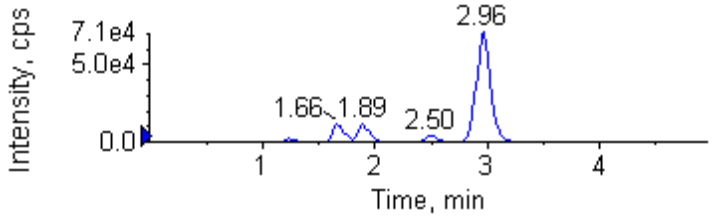

(b) LB

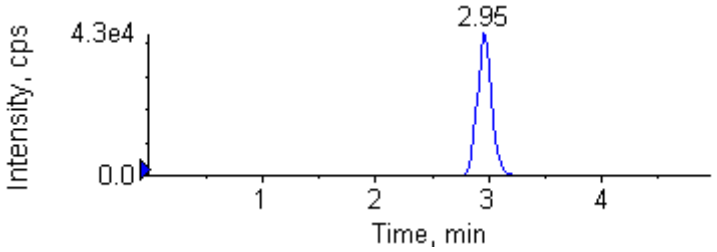

(c) M1

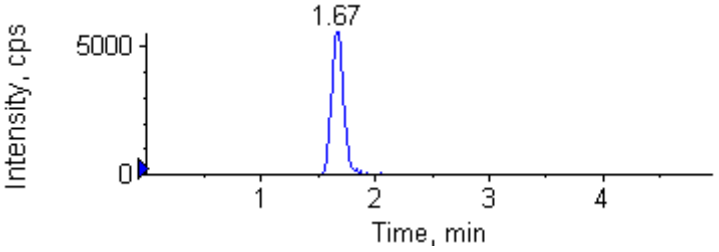

M2

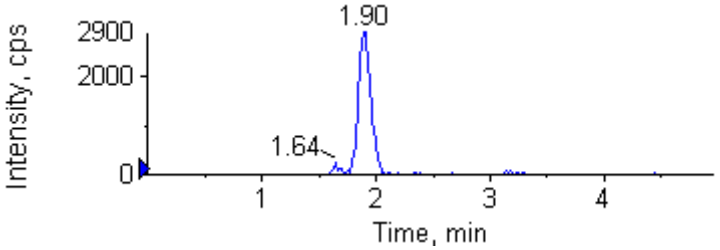

(d) M3

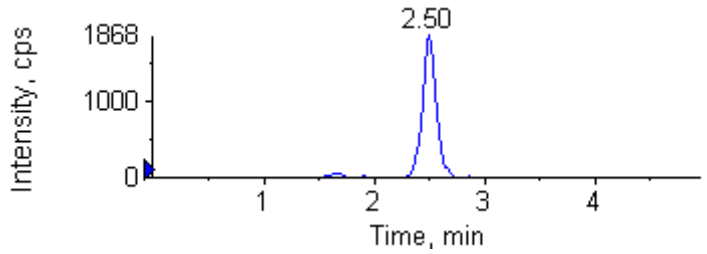

M4

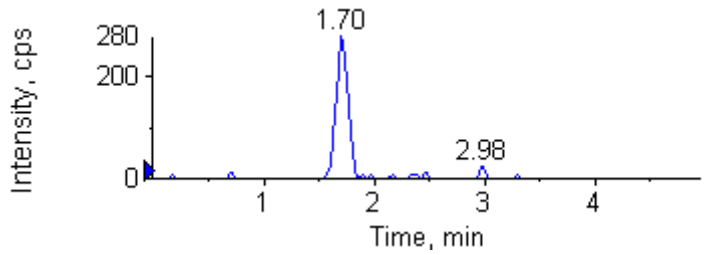

(e) M5

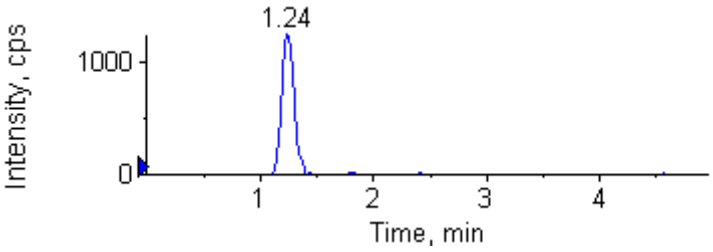

Figure 9. Representative (a) total ion chromatogram and extracted ion chromatograms from a sample of LB incubated with RLMs for 30 min using the MRM method for (b) LB (m/z 481.2); (c) demethylated LB (M1, M2; m/z 467.3); (d) hydroxylated LB (M3, M4; m/z 497.2); (e) di-demethylated LB (M5; m/z 453.1).

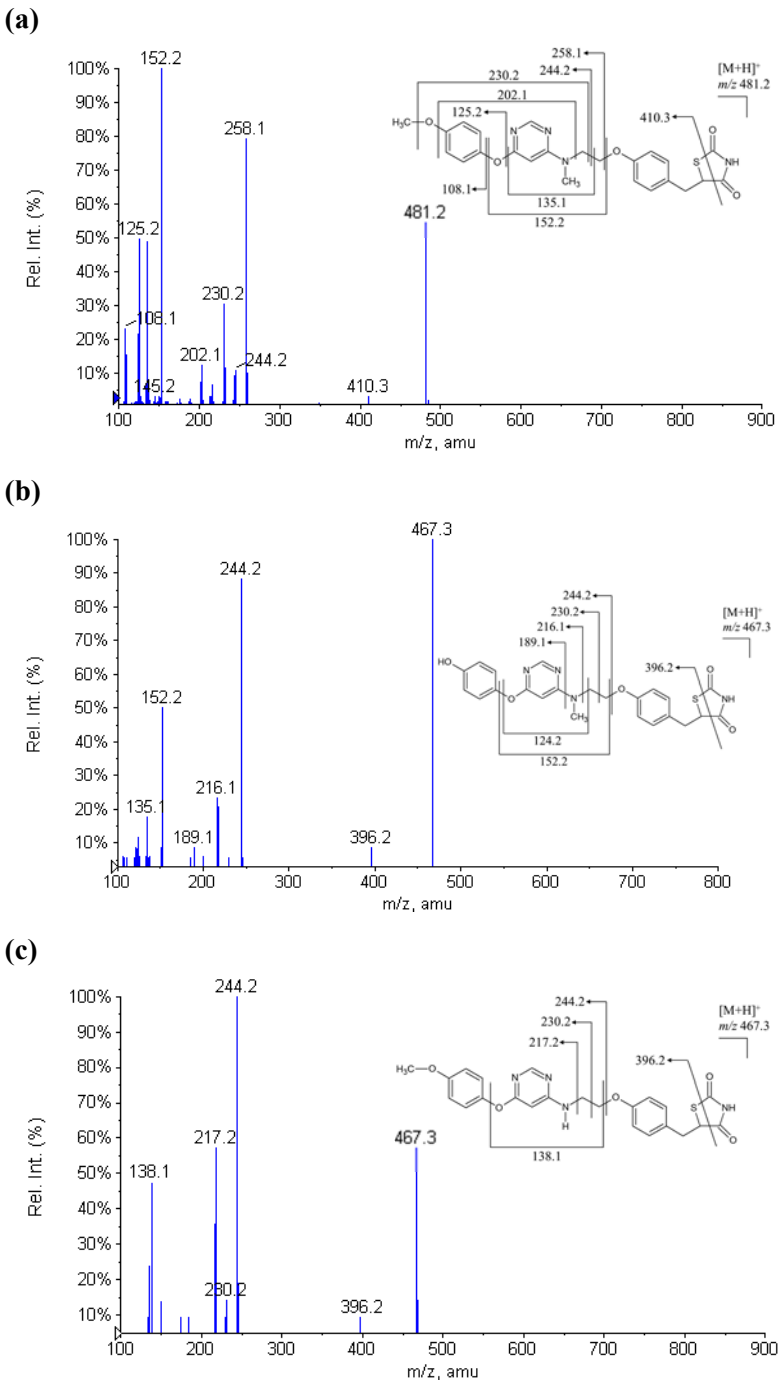

Figure 10. Enhanced product ion spectra and proposed fragmentation patterns of LB and its major metabolites detected in rat liver microsomes: (a) LB, (b) demethylated LB (M1) and (c) demethylated LB (M2).

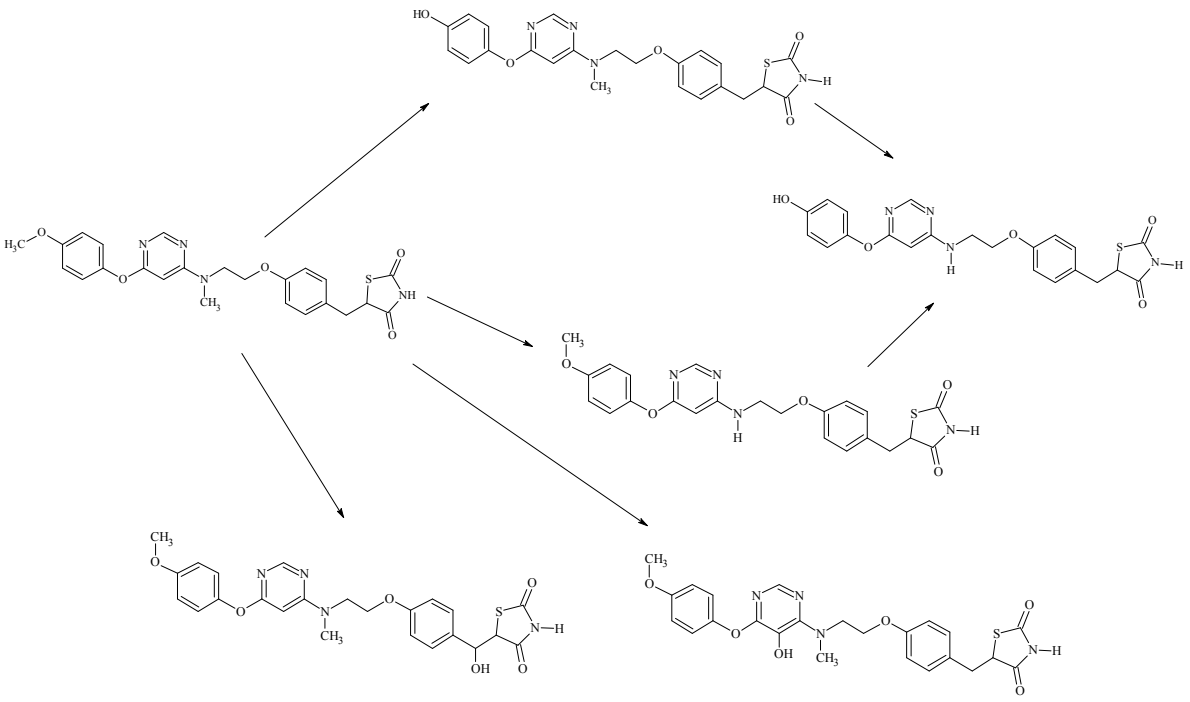

Figure 11. Proposed metabolic pathways of LB incubated with rat liver microsomes.

Table 12. Biotransformation of LB for predicted metabolites.

Biotransformation	Mass gain/loss(amu)	Predicted m/z	Formula
None (i.e., LB)	0	481.2	
oxidation	16	497.2	O
di-oxidation	32	513.2	2 × O
tri-oxidation	48	529.2	3 × O
gain of H_2O	18	499.2	H_2O
hydrogenation	2	483.2	H_2
demethylation	–14	467.3	CH_2
di-demethylation	–28	453.2	2 × CH_2
dehydrogenation	–2	479.2	H_2
sulfonation	80	561.2	SO_3
methylation	14	495.2	CH_2
di-methylation	28	509.2	2 × CH_2
methylation + oxidation	30	511.2	CH_2 + O
dimethylation + oxidation	44	525.2	2 × CH_2 + O
demethylation+oxidation	2	483.2	–1 × CH_2 + O
di-demethylation+oxidation	–12	469.2	–2 × CH_2 + O
acetylation	42	523.2	C_2H_2O
di-acetylation	84	565.2	2 × C_2H_2O

glucuronidation	176	657.2	$C_6O_6H_8$
bis-glucuronide	352.1	833.3	$2 \times C_6O_6H_8$
gluc-sulphate	256	737.2	$C_6O_6H_8SO_3$
gluc-oxidation	192	673.2	$C_6O_6H_8O$
gluc-dioxidation	208	689.2	$C_6O_6H_8 + O_2$
GSH	305.1	786.3	$C_{10}H_{15}N_3O_6S$
glucose	162.1	643.3	$C_6H_{10}O_5$

Table 13. Major MS/MS fragments of LB and its metabolites.

Biotransformation	RT (min)	$[M+H]^+$	Major fragments
None (i.e., LB)	2.95	481.2	259.2, **258.1**, 231.1, **152.2**
Demethylation (M1)	1.67	467.3	**244.2**, 216.1, **152.2**, 135.1, 111.2
Demethylation (M2)	1.90	467.3	**244.2**, 229.2, 216.1, **138.1**, 135.1,124.2
Hydroxylation (M3)	2.50	497.2	392.3, **258.2**, **152.1**
Hydroxylation (M4)	1.70	497.2	**274.2**
Di-demethylation (M5)	1.24	453.2	390.7, 286.9, 263.1, **230.2**, 125.2

3.3. *In vivo* Pharmacokinetic Studies

3.3.1. Pharmacokinetic Study of Oral and Intravenous Administrations

The mean plasma concentration-time curves in male rats following an intravenous administration of LB at doses of 0.5, 1 and 2 mg/kg are shown in Fig. 12a. The pharmacokinetic parameters, as estimated by a standard moment analysis, are listed in Table 14. The dose-normalized AUC values were determined to be 459, 514, and 481 μg · min/mL for 0.5, 1, and 2 mg/kg, respectively. Consequently, the systemic clearance showed similar values, between 1.95 and 2.19 mL/min/kg, and did not change significantly with respect to the dosage, indicating that the elimination was linear for LB in rats in the dose range studied. In addition, the V_{ss} of LB was 189 to 276 mL/kg and not statistically different with the dose, suggesting that the distribution kinetics of LB follows linear kinetics.

The mean plasma concentration-time curves in male rats following the oral administration of LB at 0.5 and 2 mg/kg are illustrated in Fig. 12b, and the pharmacokinetic parameters listed in Table 14. The T_{max} at 0.5 and 2 mg/kg was 67.5 and 48.8 min, respectively, indicating that the absorption of LB from the GI tract occurred very rapidly after its administration. The dose-normalized AUC values were 421 and 476 μg · min/mL for doses of 0.5 and 2 mg/kg, respectively, and the absolute bioavailability of LB after oral

administration was almost complete and apparently not affected by doses [i.e., 92.1% (0.5 mg/kg) and 99.0% (2 mg/kg)]. The extent of LB remaining in the gastrointestinal tract after 24 h (GI_{24h}) was negligible and exhibited values less than 0.2% of the oral dose. This suggests that the intestinal absorption of LB was complete for all doses within the range used in the present study and indicates almost complete bioavailability of LB.

The cumulative amounts of LB excreted in urine after doses of 0.5, 1 and 2 mg/kg and bile after doses of 0.5 and 1 mg/kg were determined following intravenous administration. The total recoveries of unchanged LB were 0.06-0.07% and 0.31-0.37% of the total dose for the urinary and biliary routes, respectively, which indicated that these excretory routes represent minor elimination pathways.

(a)

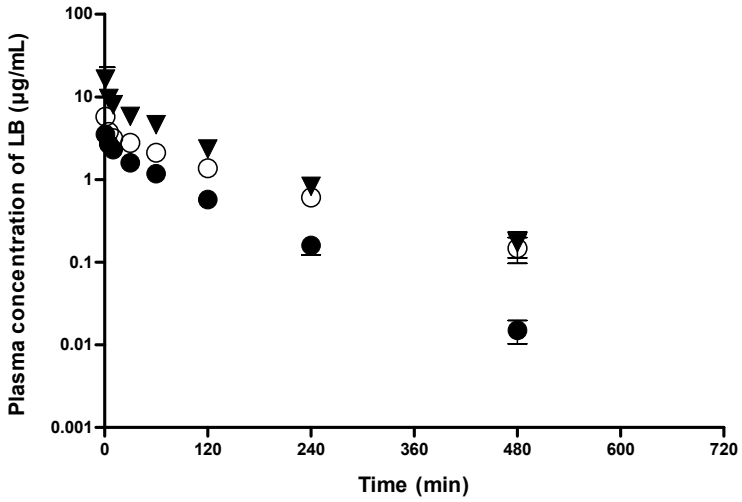

(b)

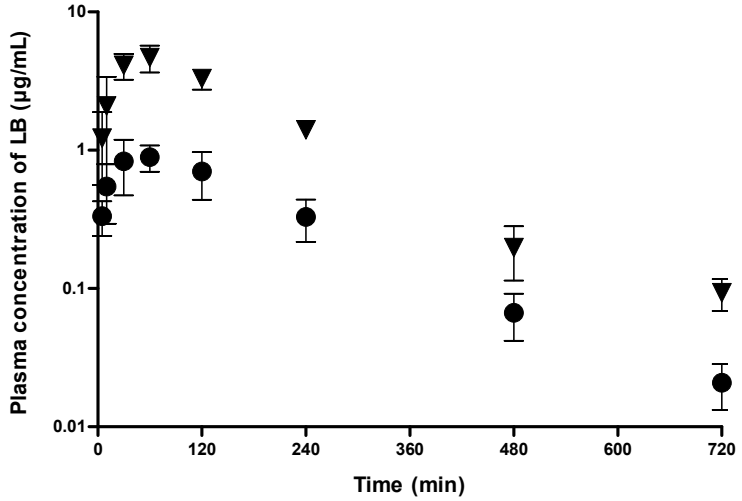

Figure 12. Temporal profiles of plasma LB concentration in rats (a) after intravenous administration at doses of 0.5 (●), 1 (○) and 2 (▼) mg/kg, and (b) after oral administration at doses of 0.5 (●) and 2 (▼) mg/kg. Data are expressed as the mean ± S.D. of quadruplicate runs.

Table 14. Pharmacokinetic parameters of LB (a) after intravenous administration at doses of 0.5, 1, and 2 mg/kg and (b) after oral administration at doses of 0.5 and 2 mg/kg in rats. Data are expressed as the mean ± S.D. of quadruplicate runs.

(a) Intravenous administration

Parameter	0.5 mg/kg	1 mg/kg	2 mg/kg
AUC_{inf} (μg·min/mL)	229 ± 18.6	514 ± 35.1	963 ± 29.6
AUC_{inf} (μg·min/mL)/Dose	459 ± 37.1	514 ± 35.1	481 ± 14.8
$t_{1/2}$ (min)	68.5 ± 6.0	110 ± 13.2	93.2 ± 13.2
MRT_{inf} (min)	85.8 ± 10.1	142 ± 16.9	108 ± 19.0
Cl (mL/min/kg)	2.19 ± 0.177	1.95 ± 0.128	2.08 ± 0.0650
Cl_r (mL/min/kg)	0.00160 ± 0.000496	0.00216 ± 0.000207	0.00187 ± 0.00123
Cl_{nr} (mL/min/kg)	2.19 ± 0.177	1.95 ± 0.128	2.08 ± 0.0638
V_{ss} (mL/kg)	189 ± 31.8	276 ± 14.0	225 ± 39.5
A_e, $urine_{0\text{-}24h}$ (% of dose)	0.0643 ± 0.0163	0.0749 ± 0.0117	0.0629 ± 0.0419
A_e, $feces_{0\text{-}24h}$ (% of dose)	1.97 ± 0.610	2.61 ± 0.417	2.19 ± 0.666
A_e, $bile_{0\text{-}24h}$ (% of dose)	0.367 ± 0.122	0.314 ± 0.133	ND[a)]
GI_{24h} (%)	0.105 ± 0.123	0.880 ± 0.0597	0.0417 ± 0.0305

a) ND: not determined.

(b) Oral administration

Parameter	0.5 mg/kg	2 mg/kg
AUC_{inf} (μg·min/mL)	211 ± 40.6	953 ± 121
AUC_{inf} (μg·min/mL) / Dose	421 ± 81.1	476 ± 60.3
C_{max} (μg/mL)	0.962 ± 0.285	4.94 ± 0.600
T_{max} (min)	67.5 ± 37.7	48.8± 22.5
A_e, $urine_{0\text{-}24h}$ (% of dose)	0.0293 ± 0.00709	0.0424 ± 0.00402
A_e, $feces_{0\text{-}24h}$ (% of dose)	9.72 ± 3.99	9.05 ± 1.80
GI_{24h} (%)	0.155 ± 0.104	0.0908 ± 0.0521
F (%)	92.1	99.0

3.3.2. Tissue Distribution

The tissue-to-plasma (T/P) ratios of LB at 1 h after the intravenous administration of 2 mg/kg in rats are shown in Fig. 13. The tissue samples were processed similar to the procedure described in section 2.2.3 and measured similar to the condition described in section 2.2.1 and 2.2.2 with good correlation coefficient within calibration range (Table 15). In general, LB was present in various tissues at concentrations above those expected from the blood remaining in the tissue. The primary distribution site for LB was the liver (i.e., T/P ratio of 5.59 ± 0.100), but it was also distributed to a lesser extent to the heart (i.e., T/P ratio of 1.68 ± 0.146), lung (i.e., T/P ratio of 1.83 ± 0.411) and fat (i.e., T/P ratio of 1.50 ± 0.172). In preliminary study, the steady state tissue to plasma ratio (K_p) value for LB was also determined in rats; the K_p values ranged from approximately 0.25-4.0 for major tissues and were comparable to the those obtained in this study.

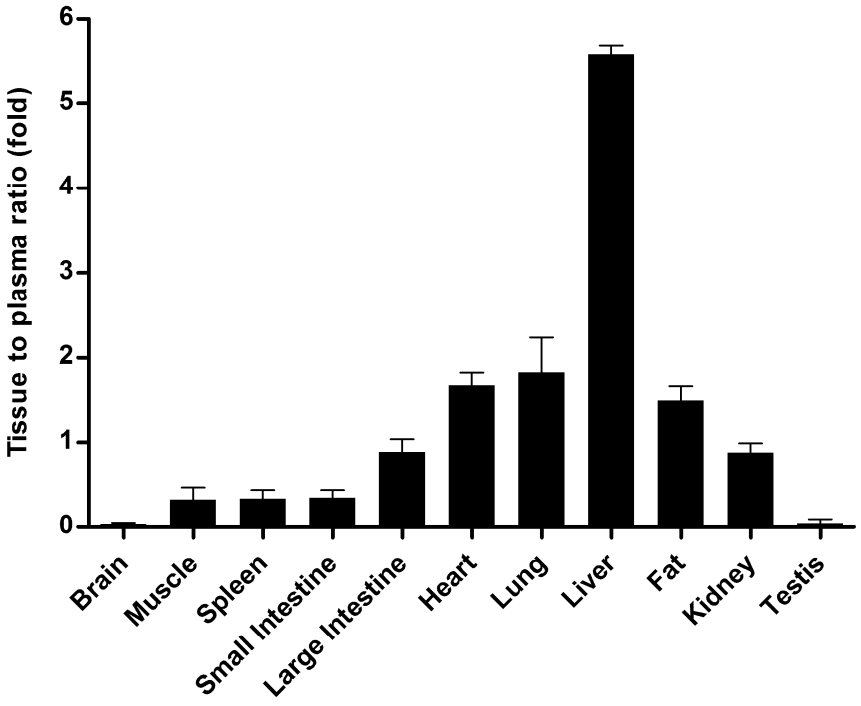

Figure 13. Tissue to plasma (T/P) concentration ratio of LB at 1 h after intravenous administration at the dose of 2 mg/kg. Data are expressed as the mean ± S.D. of quadruplicate runs.

Table 15. Regression parameters and correlation coefficients for tissue analysis.

Tissue	Calibration Range (ng/mL)	Slope	Intercept	Correlation Coefficient (r)
Brain	5-500	0.444	0.630	0.999
Muscle	20-1000	0.328	5.06	0.996
Spleen	5-1000	0.365	0.710	0.994
Small Intestine	5-1000	0.457	–0.274	0.999
Large Intestine	5-1000	0.656	–0.771	0.999
Heart	5-100	0.285	5.89	0.996
Lung	50-1000	0.308	11.6	0.992
Liver	5-1000	0.222	0.284	0.999
Fat	20-1000	0.254	–1.81	0.995
Kidney	10-1000	0.492	1.83	0.999
Testis	10-200	0.580	–0.330	0.999

3.4. Gender Differences in the Hepatic Elimination and Pharmacokinetics of LB in Rats

3.4.1. Gender Difference in the Pharmacokinetics of LB in Rats

To determine gender differences, LB was orally administered to male and female rats at doses of 0.1, 1 and 10 mg/kg; the plasma concentration-time profiles are depicted in Fig. 14. While the dose increased by a ratio of 1:10:100, the systemic exposure as measured by AUC_{last} increased by ratios of 1:19:141 for males and 1:14:118 for females (Fig. 14 and Table 16). A power model (Finn et al., 2012; Smith et al., 2000) indicated that these changes were proportional to the increase in dose (95% confidence intervals of 0.90-1.23 for males and 0.94-1.13 for females). The dose-normalized AUC_{last} for LB did not significantly differ among the doses, which suggests that LB was governed by linear kinetics.

The plasma concentrations of LB were consistently higher in female rats (Fig. 14) and, as a result, the kinetic parameters indicating systemic exposure (AUC_{last} or C_{max}) after an oral dose of LB were also consistently higher in female rats ($p<0.05$ for both AUC_{last} and C_{max}; Table 16). Nonetheless, LB extensively bound to plasma proteins regardless of gender; at a total LB concentration of 1 μM the percentage bound were 100 ± 0.0251% for males and 99.7 ± 0.0304% for females.

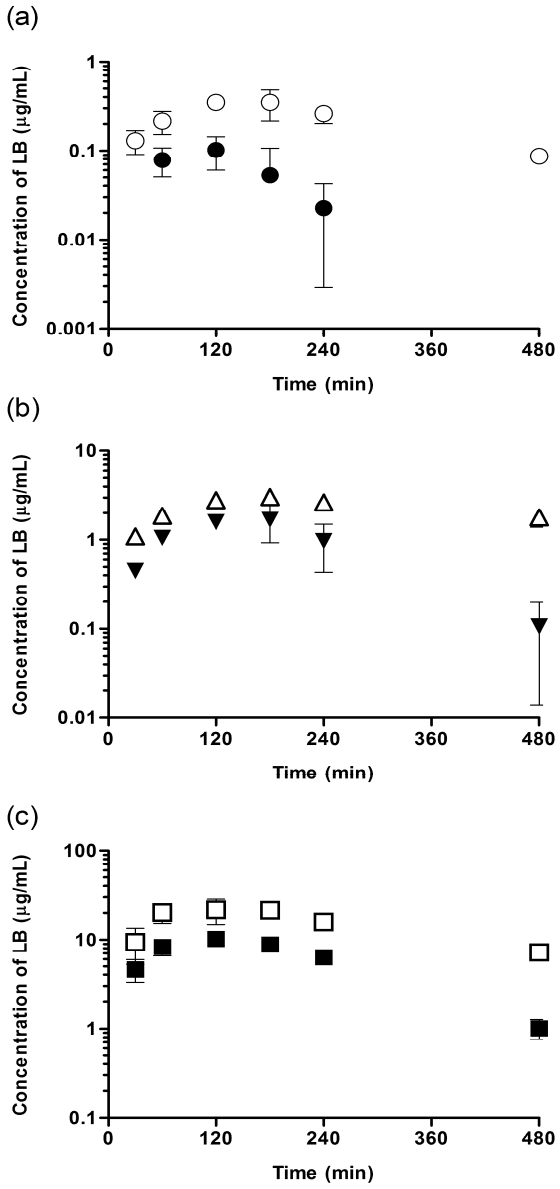

Figure 14. Mean plasma concentration-time profiles of LB after oral administration to male (filled symbol) and female (open symbol) rats at doses of 0.1 [panel (a), circle], 1 [panel (b), triangle], and 10 mg/kg [panel (c), square]. Bars are expressed as mean ± standard deviation of triplicate runs.

Table 16. Summary of pharmacokinetic parameters of LB after oral administration at doses of 0.1, 1 and 10 mg/kg in rats.

Parameter	Dose		
	0.1 mg/kg	**1 mg/kg**	**10 mg/kg**
Male rats			
AUC_{last} (μg · min/mL)	19.3 ± 5.77	367 ± 136	2730 ± 126
C_{max} (μg/mL)	0.127 ± 0.00587	1.67 ± 0.357	10.2 ± 0.201
T_{max} (min)	120 ± 0.00	150 ± 4.24	120 ± 0.00
$t_{1/2}$ (min)	62.6 ± 20.4	75.9 ± 66.0	94.4 ± 9.54
MRT (min)	134 ± 35.4	169 ± 1.31	177 ± 6.13
CL/F (mL/min/kg)	5.04 ± 1.25	2.75 ± 0.834	3.50 ± 0.199
Female rats			
AUC_{last} (μg · min/mL)	105 ± 16.0	1420 ± 586	12400 ± 1060
C_{max} (μg/mL)	0.395 ± 0.0612	3.05 ± 0.160	22.9 ± 3.21
T_{max} (min)	160 ± 34.6	140 ± 34.6	100 ± 34.6
$t_{1/2}$ (min)	162 ± 46.0	317 ± 157	192 ± 29.0
MRT (min)	203 ± 5.31	281 ± 78.7	328 ± 16.5
CL/F (mL/min/kg)	0.804 ± 0.0800	0.514 ± 0.143	0.804 ± 0.0685

3.4.2. Differences in the Metabolic Stability of LB in Rat Hepatic Microsomes

To determine whether there were gender difference in the metabolic stability of LB, liver microsomes were obtained from male and female rats. The calculated *in vitro* half-life ($t_{1/2}$) values for LB in the males and females were 18.8 ± 4.45 min and 60.7 ± 11.2 min, respectively, and the calculated microsomal CL_{int} value for LB in the male liver microsomes was much higher (0.0779 ± 0.0233 mL/min/mg protein) than in female liver microsomes (0.0233 ± 0.0039 mL/min/mg protein; $p<0.05$).

In a preliminary study using male rats, the oral absorption of LB was complete (i.e., F~1). Collectively, these observations suggest that decreased elimination rate likely underlies the changes in systemic exposure to LB. Consistent with this hypothesis, an *in vitro* metabolic stability study found that the CL_{int} value for females was approximately 29% of the value for males. Similarly, the apparent oral clearance in the female rats was approximately 20% of that the male rats but this difference was reduced by changes in the dose (Table 16).

4. DISCUSSION

The primary goal of the present study was to determine of the *in vitro* and *in vivo* properties of the absorption, distribution, metabolism, and excretion of LB, a new TZD-PPARs activator.

The extent of the absorption was first estimated using a permeability assay with artificial membranes, PAMPA. The LB permeability value corresponded to approximately 72% of its absolute oral bioavailability in humans, provided that the pre-systemic metabolism of LB was not extensive. However, it was necessary to include PEG400 (15% by volume), which is a solvent that affects permeability measurements (Sugano et al., 2001), to achieve a soluble system. In literature report (Sugano et al., 2001), when 15% PEG400 was added to the donor solution the permeability decreased to approximately 50% of the P_{app} when the PEG400 was not used. This degree of reduction appeared to be similar for all test compounds, which indicates that the decreases were primarily due to the chemicals present in the system (i.e., by affecting the partition of test compounds from the media to the lipid layer). Therefore, it appeared likely that solubilized LB itself would be more permeable to the lipid membrane and that the estimation of its bioavailability might be higher than predicted. To demonstrate this possibility, the sulfate salt of LB, a water soluble form, was found to have a PAMPA P_{app} value of 7.39

± 0.0174 × 10^{-6} cm/sec, which suggests that solubilized LB would be completely bioavailable. Consistent with this, the bioavailability of LB was also predicted to be over 94% based on the correlation between the logP value of 4.20 and bioavailability in human (Hou et al., 2007).

Based on the apical to basolateral permeability value for LB (i.e., 0.533 ± 0.0914 × 10^{-6} cm/sec) obtained in the MDCKII cell monolayer tests, it was predicted that the intestinal bioavailability of LB would be incomplete in humans. However, this contradicts the results of the PAMPA tests. In subsequent studies, it was found that the low permeability value was attributed to MDR1-mediated efflux (Table 8). The discrepancy between the permeability estimates from the PAMPA study and the cell permeability study may be related to the active efflux of LB in the apical membrane of MDCKII-MDR1 cells. In the cellular accumulation evaluation with MDR1 expressing MDCKII cells, the IC_{50} value of LB was approximately 12.5 μM in the efflux of digoxin. Although the K_m value was not reported for digoxin, MDR1 substrates typically have K_m values within the 10-100 μM range (International Transporter et al., 2010). Considering the digoxin concentration used in the inhibition study (i.e., 1 μM), the IC_{50} would be close to the K_i value for LB. Assuming the mechanism of interaction between LB and digoxin is competitive, the K_i would be regarded as reflecting the affinity of the LB for the MDR1 transporter. Because the volume of intestinal fluid in a

250 g rat is approximately 2.5 mL (Yu et al., 2009), the concentration of LB in the intestine would be expected to be approximately 104 μM and 416 μM after the oral administration of 0.5 mg/kg and 2 mg/kg of LB, respectively (Molecular weight of LB of 480.2 g/mol). Thus, the expected concentration of LB would be significantly greater than the estimated affinity of LB (viz, 12.5 μM), which in turn would mean that MDR1-mediated transport was saturated in oral administration study. Therefore, despite the fact that the drug was subjected to MDR1-mediated efflux and had an extensive efflux ratio, an oral bioavailability of more than 90% might have been possible for LB. A number of drugs with high efflux ratios, such as dicloxacillin (Smith et al., 1990) and prazocin (Bateman et al., 1979; Wempe et al., 2009), have been reported to have a relatively high oral bioavailability.

The extent of excretion to the biliary, urinary and intestinal systems were minor for LB (i.e., the combined excretion was less than 10% of the dose, Table 14). Therefore, hepatic clearance may by effectively considered systemic clearance (i.e., ~0.5 mL/min/250 g rat). Since hepatic blood flow was reported to be 14.5 mL/min for a 250 g rat (Brown et al., 1997), the hepatic extraction ratio for LB would be expected to be 0.0344 (i.e., a low extraction drug). This estimate is also consistent with the nearly complete oral bioavailability of LB, since pre-systemic elimination is not likely to occur for LB. In addition, LB appeared to interact with a number of CYP isozymes (e.g.,

1A2, 2C9 and 2C19, Table 11). In the *in vitro* metabolism study using rat liver microsomes, the reaction was primarily mediated by a phase I reaction, rather than a phase II reaction, suggesting that conjugation was not a major factor in the metabolic elimination of LB. The relatively good metabolic stability may also be related to the adequate biological half-life of LB (i.e., ~110 min, Table 14) found in the *in vivo* study.

It is generally known that the binding of drugs to plasma proteins plays an important role in the disposition of drugs. In this study, LB bound extensively to plasma proteins (i.e., up to 99.9%), and there was no appreciable concentration dependency on the unbound fraction. In particular, the extensive protein binding may also be involved in the absorption of LB. In MDCKII cell monolayer study, the efflux ratio was approximately 9.42 in wild type MDCKII cells. However, this *in vitro* estimate may be markedly different from in the *in vivo* situation, since LB primarily exists in its bound form in systemic circulation. As a result, the efflux rate for LB would be substantially lower in *in vivo* situation. This statement is consistent with the almost complete oral bioavailability of LB in rats (Table 14).

In addition to MDR1, LB also interactions with other major transporters. Of the SLC transporters studied, the interaction of LB with OATP1B3 and OAT1 resulted in IC_{50} values of over 100 μM which was the highest concentration used. For OAT3, the estimated IC_{50} was approximately 34.3

μM, suggesting that the inhibitory potential was slightly higher than those for the other two transporters. However, the plasma concentrations observed in the pharmacokinetic studies was consistently less than 20 μM (i.e., initial plasma concentration after intravenous injection of 2 mg/kg, Fig. 12a), and inhibition of the SLC transporters, except OAT3, was less likely within the concentration range in this study considering the IC_{50} of over 30 μM. LB did not appear to influence the functional activity of the OCT2 transporter at concentrations up to 100 μM. For OATP1B1, the IC_{50} values, the apparent affinity of LB, was found to be approximately 2.44 μM.

The efflux ratio of methotrexate in MDCKII-BCRP cells was only slightly lowered from 3.79 to 2.49 by the presence of LB (100 μM). In contrast, LB efflux ratio was decreased by 10-fold under similar condition with verapamil in MDCKII-BCRP cells (Table 8). Therefore, the interaction of LB with BCRP appeared to be relatively weak. Taken together with the range of plasma concentration observed in this study, these data suggest that the OATP1B1 transporter may play a kinetic role.

In this study, the total recovery of unchanged LB to the urinary, biliary, and intestinal system was less than 10 % of the administered dose, suggesting that hepatic elimination is the major route of elimination for LB. In rat liver microsomal stability study, the formation of the metabolites by demethylation

and hydroxylation after incubation of LB within rat liver microsomes was elucidated, and structure analysis of metabolites based on their product ion mass spectra resulted in identification of major metabolites as a demethylation of LB, supporting to predict the metabolites to be able to be formed in *in vivo* rat pharmacokinetic study.

Gender difference of LB in rats was observed like rosiglitazone and pioglitazone, which are TZD PPARs activators. It has been reported that rosiglitazone and pioglitazone, which are TZD PPARs activators, are primarily metabolized by CYP2C8 (Baldwin et al., 1999; Cox et al., 2000; Hanefeld, 2001). In particular, CYP2C11 is male-specific while CYP3A2 and CYP2C13 are male predominant (Imamura et al., 2002; Kato and Yamazoe, 1992; Mugford and Kedderis, 1998). Further studies will focus on a metabolic phenotyping study to provide more information for LB. At present, it is not clear whether the gender differences in the pharmacokinetics of LB can be extrapolated to humans. However, it appears the oral clearances of some TZD PPARs activators including rosiglitazone and pioglitazone are slower in women (Malinowski and Bolesta, 2000; Patel et al., 1999). This finding is consistent with the results of the animal studies (Beconi et al., 2003; Fujita et al., 2003).

In summary, LB, a new drug candidate for the use as an activator of TZD-PPAR, showed linear pharmacokinetics in terms of absorption, tissue

distribution, and elimination in rats. LB had a nearly complete bioavailability in rats despite the fact that it may be subjected to MDR1-mediated efflux *in vitro*. The discrepancy in LB kinetics may be attributed to a number of reasons including the high affinity of LB for MDR1, the extensive protein binding of LB in the plasma, and/or high lipophilicity. Of the other six major SLC transporters, OATP1B1 is likely to have kinetic relevance considering the *in vivo* concentration levels found in this study. LB appeared to have a reasonably long metabolic half-life, primarily via CYP dependent processes (viz, CYP1A2, 2C9 and 2C19). The formation of the metabolites by demethylation and hydroxylation of LB in rat liver microsomes was elucidated, supporting to predict the metabolites to be able to be formed in *in vivo* rat pharmacokinetic study. Additionally, the gender difference was shown in the pharmacokinetics and hepatic metabolism for LB in rats.

5. REFERENCES

Adams, M., Montague, C.T., Prins, J.B., Holder, J.C., Smith, S.A., Sanders, L., Digby, J.E., Sewter, C.P., Lazar, M.A., Chatterjee, V.K., O'Rahilly, S., 1997. Activators of peroxisome proliferator-activated receptor gamma have depot-specific effects on human preadipocyte differentiation. Journal of Clinical Investigation 100, 3149-3153.

Anderson, L.A., McTernan, P.G., Barnett, A.H., Kumar, S., 2001. The effects of androgens and estrogens on preadipocyte proliferation in human adipose tissue: influence of gender and site. Journal of Clinical Endocrinology and Metabolism 86, 5045-5051.

Aslamkhan, A.G., Han, Y.H., Yang, X.P., Zalups, R.K., Pritchard, J.B., 2003. Human renal organic anion transporter 1-dependent uptake and toxicity of mercuric-thiol conjugates in Madin-Darby canine kidney cells. Molecular Pharmacology 63, 590-596.

Association, A.D., 2010. Diagnosis and classification of diabetes mellitus. Diabetes Care 33, S62-S69.

Baillie, T.A., 2006. Future of toxicology-metabolic activation and drug design: challenges and opportunities in chemical toxicology. Chemical Research in Toxicology 19, 889-893.

Baillie, T.A., 2009. Approaches to the assessment of stable and chemically reactive drug metabolites in early clinical trials. Chemical Research in Toxicology 22, 263-266.

Baldwin, S.J., Clarke, S.E., Chenery, R.J., 1999. Characterization of the cytochrome P450 enzymes involved in the in vitro metabolism of rosiglitazone. British Journal of Clinical Pharmacology 48, 424-432.

Baranczewski, P., Stanczak, A., Sundberg, K., Svensson, R., Wallin, A., Jansson, J., Garberg, P., Postlind, H., 2006. Introduction to in vitro estimation of metabolic stability and drug interactions of new chemical entities in drug discovery and development. Pharmacological Reports 58, 453-472.

Bateman, D.N., Hobbs, D.C., Twomey, T.M., Stevens, E.A., Rawlins, M.D., 1979. Prazosin, pharmacokinetics and concentration effect. European Journal of Clinical Pharmacology 16, 177-181.

Baughman, T.M., Graham, R.A., Wells-Knecht, K., Silver, I.S., Tyler, L.O., Wells-Knecht, M., Zhao, Z., 2005. Metabolic activation of pioglitazone identified from rat and human liver microsomes and freshly isolated hepatocytes. Drug Metabolism and Disposition 33, 733-738.

Beconi, M., Mao, A., Creighton, M., Hop, C.E., Chiu, S.H., Eydelloth, R., Franklin, R., Tang, F., Yu, N., Vincent, S., 2003. Species and gender differences in the formation of an active metabolite of a substituted 2,4-thiazolidinedione insulin sensitizer. Xenobiotica 33, 767-787.

Benet, L.Z., 1978. Effect of route of administration and distribution on drug action. Journal of Pharmacokinetics and Biopharmaceutics 6, 559-585.

Benz, V., Kintscher, U., Foryst-Ludwig, A., 2012. Sex-specific differences in Type 2 Diabetes Mellitus and dyslipidemia therapy: PPAR agonists. Handbook of Experimental Pharmacology, 387-410.

Brandoni, A., Anzai, N., Kanai, Y., Endou, H., Torres, A.M., 2006. Renal elimination of p-aminohippurate (PAH) in response to three days of biliary obstruction in the rat. The role of OAT1 and OAT3. Biochimica et Biophysica Acta 1762, 673-682.

Brown, R.P., Delp, M.D., Lindstedt, S.L., Rhomberg, L.R., Beliles, R.P., 1997. Physiological parameter values for physiologically based pharmacokinetic models. Toxicology and Industrial Health 13, 407-484.

Caldwell, G.W., Yan, Z., Tang, W., Dasgupta, M., Hasting, B., 2009. ADME optimization and toxicity assessment in early- and late-phase drug discovery. Current Topics in Medicinal Chemistry 9, 965-980.

Chaturvedi, P.R., Decker, C.J., Odinecs, A., 2001. Prediction of pharmacokinetic properties using experimental approaches during early drug discovery. Current Opinion in Chemical Biology 5, 452-463.

Commandeur, J., Stijntjes, G.J., Vermeulen, N., 1995. Enzymes and transport systems involved in the formation and disposition of glutathione S-conjugates.

Role in bioactivation and detoxication mechanisms of xenobiotics. Pharmacological Reviews 47, 271-330.

Cox, P.J., Ryan, D.A., Hollis, F.J., Harris, A.M., Miller, A.K., Vousden, M., Cowley, H., 2000. Absorption, disposition, and metabolism of rosiglitazone, a potent thiazolidinedione insulin sensitizer, in humans. Drug Metabolism and Disposition 28, 772-780.

DiMasi, J.A., 2001. Risks in new drug development: approval success rates for investigational drugs. Clinical Pharmacology and Therapeutics 69, 297-307.

Feng, B., Mills, J.B., Davidson, R.E., Mireles, R.J., Janiszewski, J.S., Troutman, M.D., de Morais, S.M., 2008. In vitro P-glycoprotein assays to predict the in vivo interactions of P-glycoprotein with drugs in the central nervous system. Drug Metabolism and Disposition 36, 268-275.

Ferre, P., 2004. The biology of peroxisome proliferator-activated receptors: relationship with lipid metabolism and insulin sensitivity. Diabetes 53, S43-S50.

Finn, A.L., Vasisht, N., Stark, J.G., Gever, L.N., Tagarro, I., 2012. Dose proportionality and pharmacokinetics of fentanyl buccal soluble film in healthy subjects: a phase I, open-label, three-period, crossover study. Clinical Drug Investigation 32, 63-71.

Fujita, T., Urban, T.J., Leabman, M.K., Fujita, K., Giacomini, K.M., 2006. Transport of drugs in the kidney by the human organic cation transporter, OCT2 and its genetic variants. Journal of Pharmaceutical Sciences 95, 25-36.

Fujita, Y., Yamada, Y., Kusama, M., Yamauchi, T., Kamon, J., Kadowaki, T., Iga, T., 2003. Sex differences in the pharmacokinetics of pioglitazone in rats. Comparative biochemistry and physiology. Toxicology & Pharmacology 136, 85-94.

Furge, L.L., Guengerich, F.P., 2006. Cytochrome P450 enzymes in drug metabolism and chemical toxicology: An introduction. Biochemistry and Molecular Biology Education 34, 66-74.

Gibaldi, M., Perrier, D., 1982. Pharmacokinetics, Second Edition. Taylor & Francis.

Guengerich, F.P., 2008. Cytochrome P450 and chemical toxicology. Chemical Research in Toxicology 21, 70-83.

Hanefeld, M., 2001. Pharmacokinetics and clinical efficacy of pioglitazone. International Journal of Clinical Practice, 19-25.

Harris, M.I., Flegal, K.M., Cowie, C.C., Eberhardt, M.S., Goldstein, D.E., Little, R.R., Wiedmeyer, H.M., Byrd-Holt, D.D., 1998. Prevalence of diabetes, impaired fasting glucose, and impaired glucose tolerance in U.S. adults. The Third National Health and Nutrition Examination Survey, 1988-1994. Diabetes Care 21, 518-524.

Hevener, A.L., Olefsky, J.M., Reichart, D., Nguyen, M.T., Bandyopadyhay, G., Leung, H.Y., Watt, M.J., Benner, C., Febbraio, M.A., Nguyen, A.K., Folian, B., Subramaniam, S., Gonzalez, F.J., Glass, C.K., Ricote, M., 2007. Macrophage PPAR gamma is required for normal skeletal muscle and hepatic insulin sensitivity and full antidiabetic effects of thiazolidinediones. Journal of Clinical Investigation 117, 1658-1669.

Hou, T., Wang, J., Zhang, W., Xu, X., 2007. ADME evaluation in drug discovery. 7. Prediction of oral absorption by correlation and classification. Journal of Chemical Information and Modeling 47, 208-218.

Huang, L., Berry, L., Ganga, S., Janosky, B., Chen, A., Roberts, J., Colletti, A.E., Lin, M.H., 2010. Relationship between passive permeability, efflux, and predictability of clearance from in vitro metabolic intrinsic clearance. Drug Metabolism and Disposition 38, 223-231.

Imamura, Y., Kaneko, M., Takada, H., Otagiri, M., Shimada, H., Akita, H., 2002. Sex-dependent pharmacokinetics of S(-)-hydroxyhexamide, a pharmacologically active metabolite of acetohexamide, in rats. Comparative Biochemistry and Physiology 133, 587-592.

International Transporter, C., Giacomini, K.M., Huang, S.M., Tweedie, D.J., Benet, L.Z., Brouwer, K.L., Chu, X., Dahlin, A., Evers, R., Fischer, V., Hillgren, K.M., Hoffmaster, K.A., Ishikawa, T., Keppler, D., Kim, R.B., Lee, C.A., Niemi, M., Polli, J.W., Sugiyama, Y., Swaan, P.W., Ware, J.A., Wright,

S.H., Yee, S.W., Zamek-Gliszczynski, M.J., Zhang, L., 2010. Membrane transporters in drug development. Nature reviews. Drug Discovery 9, 215-236.

Irvine, J.D., Takahashi, L., Lockhart, K., Cheong, J., Tolan, J.W., Selick, H.E., Grove, J.R., 1999. MDCK (Madin-Darby canine kidney) cells: A tool for membrane permeability screening. Journal of Pharmaceutical Sciences 88, 28-33.

Izumi, S., Nozaki, Y., Komori, T., Maeda, K., Takenaka, O., Kusano, K., Yoshimura, T., Kusuhara, H., Sugiyama, Y., 2013. Substrate-dependent inhibition of organic anion transporting polypeptide 1B1: comparative analysis with prototypical probe substrates estradiol-17beta-glucuronide, estrone-3-sulfate, and sulfobromophthalein. Drug Metabolism and Disposition 41, 1859-1866.

Jay, M.A., Ren, J., 2007. Peroxisome proliferator-activated receptor (PPAR) in metabolic syndrome and type 2 diabetes mellitus. Current Diabetes Reviews 3, 33-39.

Kato, R., Yamazoe, Y., 1992. Sex-specific cytochrome P450 as a cause of sex- and species-related differences in drug toxicity. Toxicology Letters 64-65, 661-667.

Kerns, E.H., Di, L., Petusky, S., Farris, M., Ley, R., Jupp, P., 2004. Combined application of parallel artificial membrane permeability assay and Caco-2

permeability assays in drug discovery. Journal of Pharmaceutical Sciences 93, 1440-1453.

Kim, B.Y., Ahn, J.B., Lee, H.W., Kang, S.K., Lee, J.H., Shin, J.S., Ahn, S.K., Hong, C.I., Yoon, S.S., 2004. Synthesis and biological activity of novel substituted pyridines and purines containing 2,4-thiazolidinedione. European Journal of Medicinal Chemistry 39, 433-447.

Kim, B.Y., Ahn, J.B., Lee, H.W., Moon, K.S., Sim, T.B., Shin, J.S., Ahn, S.K., Hong, C.I., 2003. Synthesis and antihyperglycemic activity of erythrose, ribose and substituted pyrrolidine containing thiazolidinedione derivatives. Chemical & Pharmaceutical Bulletin 51, 276-285.

Kim, J.W., Kim, J.R., Yi, S., Shin, K.H., Shin, H.S., Yoon, S.H., Cho, J.Y., Kim, D.H., Shin, S.G., Jang, I.J., Yu, K.S., 2011. Tolerability and pharmacokinetics of lobeglitazone (CKD-501), a peroxisome proliferator-activated receptor-gamma agonist: a single- and multiple-dose, double-blind, randomized control study in healthy male Korean subjects. Clinical Therapeutics 33, 1819-1830.

Kim, M.H., Maeng, H.J., Yu, K.H., Lee, K.R., Tsuruo, T., Kim, D.D., Shim, C.K., Chung, S.J., 2010. Evidence of carrier-mediated transport in the penetration of donepezil into the rat brain. Journal of Pharmaceutical Sciences 99, 1548-1566.

Kindla, J., Muller, F., Mieth, M., Fromm, M.F., Konig, J., 2011. Influence of non-steroidal anti-inflammatory drugs on organic anion transporting polypeptide (OATP) 1B1- and OATP1B3-mediated drug transport. Drug Metabolism and Disposition 39, 1047-1053.

Kurihara, A., Suzuki, H., Sawada, Y., Sugiyama, Y., Iga, T., Hanano, M., 1988. Transport of digoxin into brain microvessels and choroid plexuses isolated from guinea pig. Journal of Pharmaceutical Sciences 77, 347-352.

Lee, H.W., Ahn, J.B., Kang, S.K., Ahn, S.K., Ha, D.-C., 2007. Process development and scale-up of PPAR α/γ dual agonist lobeglitazone sulfate (CKD-501). Organic Process Research & Development 11, 190-199.

Lee, H.W., Kim, B.Y., Ahn, J.B., Kang, S.K., Lee, J.H., Shin, J.S., Ahn, S.K., Lee, S.J., Yoon, S.S., 2005. Molecular design, synthesis, and hypoglycemic and hypolipidemic activities of novel pyrimidine derivatives having thiazolidinedione. European Journal of Medicinal Chemistry 40, 862-874.

Lee, J.H., Woo, Y.A., Hwang, I.C., Kim, C.Y., Kim, D.D., Shim, C.K., Chung, S.J., 2009. Quantification of CKD-501, lobeglitazone, in rat plasma using a liquid-chromatography/tandem mass spectrometry method and its applications to pharmacokinetic studies. Journal of Pharmaceutical and Biomedical Analysis 50, 872-877.

Legraverend, C., Mode, A., Westin, S., Strom, A., Eguchi, H., Zaphiropoulos, P.G., Gustafsson, J.A., 1992. Transcriptional regulation of rat P-450 2C gene

subfamily members by the sexually dimorphic pattern of growth hormone secretion. Molecular Endocrinology 6, 259-266.

Lennard, M.S., 1993. Genetically determined adverse drug reactions involving metabolism. Drug Safety 9, 60-77.

Li, D., Au, J.L., 2001. Mdr1 transfection causes enhanced apoptosis by paclitaxel: an effect independent of drug efflux function of P-glycoprotein. Pharmaceutical Research 18, 907-913.

Loi, C.M., Young, M., Randinitis, E., Vassos, A., Koup, J.R., 1999. Clinical pharmacokinetics of troglitazone. Clinical Pharmacokinetics 37, 91-104.

MacKellar, J., Cushman, S.W., Periwal, V., 2009. Differential effects of thiazolidinediones on adipocyte growth and recruitment in Zucker fatty rats. PloS One 4, e8196.

Malinowski, J.M., Bolesta, S., 2000. Rosiglitazone in the treatment of type 2 diabetes mellitus: a critical review. Clinical Therapeutics 22, 1151-1168.

Mallet, C.R., Lu, Z., Fisk, R., Mazzeo, J.R., Neue, U.D., 2003. Performance of an ultra-low elution-volume 96-well plate: drug discovery and development applications. Rapid Communications in Mass Spectrometry 17, 163-170.

Matsushima, S., Maeda, K., Kondo, C., Hirano, M., Sasaki, M., Suzuki, H., Sugiyama, Y., 2005. Identification of the hepatic efflux transporters of organic anions using double-transfected Madin-Darby canine kidney II cells

expressing human organic anion-transporting polypeptide 1B1 (OATP1B1)/multidrug resistance-associated protein 2, OATP1B1/multidrug resistance 1, and OATP1B1/breast cancer resistance protein. Journal of Pharmacology and Experimental Therapeutics 314, 1059-1067.

Matuszewski, B.K., Constanzer, M.L., Chavez-Eng, C.M., 2003. Strategies for the assessment of matrix effect in quantitative bioanalytical methods based on HPLC-MS/MS. Analytical Chemistry 75, 3019-3030.

Mori, Y., Murakawa, Y., Okada, K., Horikoshi, H., Yokoyama, J., Tajima, N., Ikeda, Y., 1999. Effect of troglitazone on body fat distribution in type 2 diabetic patients. Diabetes Care 22, 908-912.

Mugford, C.A., Kedderis, G.L., 1998. Sex-dependent metabolism of xenobiotics. Drug Metabolism Reviews 30, 441-498.

Muller, C., Goubin, F., Ferrandis, E., Cornil-Scharwtz, I., Bailly, J.D., Bordier, C., Benard, J., Sikic, B.I., Laurent, G., 1995. Evidence for transcriptional control of human mdr1 gene expression by verapamil in multidrug-resistant leukemic cells. Molecular Pharmacology 47, 51-56.

Norgren, S., Arner, P., Luthman, H., 1994. Insulin receptor ribonucleic acid levels and alternative splicing in human liver, muscle, and adipose tissue: tissue specificity and relation to insulin action. Journal of Clinical Endocrinology and Metabolism 78, 757-762.

Obach, R.S., Baxter, J.G., Liston, T.E., Silber, B.M., Jones, B.C., MacIntyre, F., Rance, D.J., Wastall, P., 1997. The prediction of human pharmacokinetic parameters from preclinical and in vitro metabolism data. Journal of Pharmacology and Experimental Therapeutics 283, 46-58.

Orasanu, G., Ziouzenkova, O., Devchand, P.R., Nehra, V., Hamdy, O., Horton, E.S., Plutzky, J., 2008. The peroxisome proliferator-activated receptor-gamma agonist pioglitazone represses inflammation in a peroxisome proliferator-activated receptor-alpha-dependent manner in vitro and in vivo in mice. Journal of the American College of Cardiology 52, 869-881.

Pang, K.S., Rowland, M., 1977. Hepatic clearance of drugs. I. Theoretical considerations of a "well-stirred" model and a "parallel tube" model. Influence of hepatic blood flow, plasma and blood cell binding, and the hepatocellular enzymatic activity on hepatic drug clearance. Journal of Pharmacokinetics and Biopharmaceutics 5, 625-653.

Park, B.K., Kitteringham, N.R., Kenny, J.R., Pirmohamed, M., 2001. Drug metabolism and drug toxicity. Inflammopharmacology 9, 183-199.

Patel, J., Anderson, R.J., Rappaport, E.B., 1999. Rosiglitazone monotherapy improves glycaemic control in patients with type 2 diabetes: a twelve-week, randomized, placebo-controlled study. Diabetes, Obesity & Metabolism 1, 165-172.

Prakash, C., Sharma, R., Gleave, M., Nedderman, A., 2008. In vitro screening techniques for reactive metabolites for minimizing bioactivation potential in drug discovery. Current Drug Metabolism 9, 952-964.

Prueksaritanont, T., Chu, X., Gibson, C., Cui, D., Yee, K.L., Ballard, J., Cabalu, T., Hochman, J., 2013. Drug-drug interaction studies: regulatory guidance and an industry perspective. AAPS J 15, 629-645.

Rouan, M.C., Buffet, C., Marfil, F., Humbert, H., Maurer, G., 2001. Plasma deproteinization by precipitation and filtration in the 96-well format. Journal of Pharmaceutical and Biomedical Analysis 25, 995-1000.

Sauerberg, P., Bury, P.S., Mogensen, J.P., Deussen, H.J., Pettersson, I., Fleckner, J., Nehlin, J., Frederiksen, K.S., Albrektsen, T., Din, N., Svensson, L.A., Ynddal, L., Wulff, E.M., Jeppesen, L., 2003. Large dimeric ligands with favorable pharmacokinetic properties and peroxisome proliferator-activated receptor agonist activity in vitro and in vivo. Journal of Medicinal Chemistry 46, 4883-4894.

Schinkel, A.H., Mayer, U., Wagenaar, E., Mol, C.A., van Deemter, L., Smit, J.J., van der Valk, M.A., Voordouw, A.C., Spits, H., van Tellingen, O., Zijlmans, J.M., Fibbe, W.E., Borst, P., 1997. Normal viability and altered pharmacokinetics in mice lacking mdr1-type (drug-transporting) P-glycoproteins. Proceedings of the National Academy of Sciences of the United States of America 94, 4028-4033.

Shapiro, B.H., Agrawal, A.K., Pampori, N.A., 1995. Gender differences in drug metabolism regulated by growth hormone. International Journal of Biochemistry & Cell Biology 27, 9-20.

Skett, P., 1988. Biochemical basis of sex differences in drug metabolism. Pharmacology & Therapeutics 38, 269-304.

Smith, A.L., Meeks, C.A., Koup, J.R., Opheim, K.E., Weber, A., Vishwanathan, C.T., 1990. Dicloxacillin absorption and elimination in children. Developmental Pharmacology and Therapeutics 14, 35-44.

Smith, B.P., Vandenhende, F.R., DeSante, K.A., Farid, N.A., Welch, P.A., Callaghan, J.T., Forgue, S.T., 2000. Confidence interval criteria for assessment of dose proportionality. Pharmaceutical Research 17, 1278-1283.

Soldin, O.P., Chung, S.H., Mattison, D.R., 2011. Sex differences in drug disposition. Journal of Biomedicine & Biotechnology 2011, 187103.

Soldner, A., Benet, L.Z., Mutschler, E., Christians, U., 2000. Active transport of the angiotensin-II antagonist losartan and its main metabolite EXP 3174 across MDCK-MDR1 and caco-2 cell monolayers. British Journal of Pharmacology 129, 1235-1243.

Song, S., Suzuki, H., Kawai, R., Sugiyama, Y., 1999. Effect of PSC 833, a P-glycoprotein modulator, on the disposition of vincristine and digoxin in rats. Drug Metabolism and Disposition 27, 689-694.

Sugano, K., Hamada, H., Machida, M., Ushio, H., Saitoh, K., Terada, K., 2001. Optimized conditions of bio-mimetic artificial membrane permeation assay. International Journal of Pharmaceutics 228, 181-188.

Sun, H., Scott, D.O., 2010. Structure-based drug metabolism predictions for drug design. Chemical Biology & Drug Design 75, 3-17.

Tang, W., Lu, A.Y., 2009. Drug metabolism and pharmacokinetics in support of drug design. Current Pharmaceutical Design 15, 2170-2183.

Treiber, A., Schneiter, R., Hausler, S., Stieger, B., 2007. Bosentan is a substrate of human OATP1B1 and OATP1B3: inhibition of hepatic uptake as the common mechanism of its interactions with cyclosporin A, rifampicin, and sildenafil. Drug Metabolism and Disposition 35, 1400-1407.

Ueki, M., Galonic, D.P., Vaillancourt, F.H., Garneau-Tsodikova, S., Yeh, E., Vosburg, D.A., Schroeder, F.C., Osada, H., Walsh, C.T., 2006. Enzymatic generation of the antimetabolite gamma,gamma-dichloroaminobutyrate by NRPS and mononuclear iron halogenase action in a streptomycete. Chemistry & Biology 13, 1183-1191.

Umehara, K.I., Iwatsubo, T., Noguchi, K., Usui, T., Kamimura, H., 2008. Effect of cationic drugs on the transporting activity of human and rat OCT/Oct 1-3 in vitro and implications for drug-drug interactions. Xenobiotica 38, 1203-1218.

Uwai, Y., Okuda, M., Takami, K., Hashimoto, Y., Inui, K., 1998. Functional characterization of the rat multispecific organic anion transporter OAT1 mediating basolateral uptake of anionic drugs in the kidney. FEBS Letters 438, 321-324.

Vlckova, V., Cornelius, V., Kasliwal, R., Wilton, L., Shakir, S., 2010. Hypoglycaemia with pioglitazone: analysis of data from the prescription-event monitoring study. Journal of Evaluation in Clinical Practice 16, 1124-1128.

Walker, D., Brady, J., Dalvie, D., Davis, J., Dowty, M., Duncan, J.N., Nedderman, A., Obach, R.S., Wright, P., 2009. A holistic strategy for characterizing the safety of metabolites through drug discovery and development. Chemical Research in Toxicology 22, 1653-1662.

Walter, R.E., Cramer, J.A., Tse, F.L., 2001. Comparison of manual protein precipitation (PPT) versus a new small volume PPT 96-well filter plate to decrease sample preparation time. Journal of Pharmaceutical and Biomedical Analysis 25, 331-337.

Waxman, D.J., 1992. Regulation of liver-specific steroid metabolizing cytochromes P450: cholesterol 7alpha-hydroxylase, bile acid 6beta-hydroxylase, and growth hormone-responsive steroid hormone hydroxylases. Journal of Steroid Biochemistry and Molecular Biology 43, 1055-1072.

Wempe, M.F., Wright, C., Little, J.L., Lightner, J.W., Large, S.E., Caflisch, G.B., Buchanan, C.M., Rice, P.J., Wacher, V.J., Ruble, K.M., Edgar, K.J., 2009. Inhibiting efflux with novel non-ionic surfactants: rational design based on vitamin E TPGS. International Journal of Pharmaceutics 370, 93-102.

Williams, J.A., Hyland, R., Jones, B.C., Smith, D.A., Hurst, S., Goosen, T.C., Peterkin, V., Koup, J.R., Ball, S.E., 2004. Drug-drug interactions for UDP-glucuronosyltransferase substrates: a pharmacokinetic explanation for typically observed low exposure (AUCi/AUC) ratios. Drug Metabolism and Disposition 32, 1201-1208.

Windass, A.S., Lowes, S., Wang, Y., Brown, C.D., 2007. The contribution of organic anion transporters OAT1 and OAT3 to the renal uptake of rosuvastatin. Journal of Pharmacology and Experimental Therapeutics 322, 1221-1227.

Wysowski, D.K., Swartz, L., 2005. Adverse drug event surveillance and drug withdrawals in the United States, 1969-2002: the importance of reporting suspected reactions. Archives of Internal Medicine 165, 1363-1369.

Yu, K.H., Lee, Y.R., Ahn, S.H., Kim, D.D., Shim, C.K., Chung, S.J., 2009. Contribution of a significant first-pass effect of dimethyl-4,4'-dimethoxy-5,6,5',6'-dimethylene dioxybiphenyl-2,2'-dicarboxylate in the liver to its poor bioavailability in rats. Journal of Pharmacy and Pharmacology 61, 1197-1203.

Zhang, Z., Zhu, M., Tang, W., 2009. Metabolite identification and profiling in drug design: current practice and future directions. Current Pharmaceutical Design 15, 2220-2235.

Zhu, C., Jiang, L., Chen, T.M., Hwang, K.K., 2002. A comparative study of artificial membrane permeability assay for high throughput profiling of drug absorption potential. European Journal of Medicinal Chemistry 37, 399-407.

Zhu, M., Zhang, D., Zhang, H., Shyu, W.C., 2009. Integrated strategies for assessment of metabolite exposure in humans during drug development: analytical challenges and clinical development considerations. Biopharmaceutics & Drug Disposition 30, 163-184.

6. 국문초록

본 연구는 peroxisome proliferator-activated receptor (PPAR)-γ 활성제로 개발된 thiazolidinedione (TZD)계열 약물 Lobeglitazone (LB)의 흡수, 분포, 대사 및 배설에 대한 체내 동태를 평가하는 것이다. LB 는 parallel artificial membrane permeability assay (PAMPA)와 Madin-Darby canine kidney (MDCK) cell monolayer 를 이용한 투과실험에서 높은 생체이용률이 예측되었다. MDCKII-MDR1 cell monolayer 를 이용한 실험에서, LB 의 apical-to-basolateral (A to B) transport 는 wild type 과 큰 차이가 없었으나, basolateral-to-apical (B to A) transport 는 통계학적으로 유의성있게 증가하여 MDR1 transporter 가 관여함을 알 수 있었고, inhibitor 로 전처리시 efflux ratio 가 감소하여 MDR1 efflux transporter 의 기질 (substrate)인 것을 확인하였다. 또한, MDCKII-MDR1 cell 에서 digoxin 의 efflux 를 억제하는 LB 의 농도 (IC_{50})는 약 12.5 μM 이었으며, MDCKII-BCRP cell monolayer 실험에서 BCRP transporter 는 LB 수송과는 관련이 적었다. OATP1B1, OATP1B3, OAT1 및 OAT3 transporter 에 대한 LB 의 IC_{50} 는 2.44, 216, 151 및 34.3

μM 이었으며, 이러한 결과는 2 mg/kg 용량으로 정맥투여한 랫드의 혈중농도 범위를 고려해 볼 때, LB 가 OATP1B1 transporter 와 상호작용 (interaction)할 것으로 사료되었다.

랫드 간 마이크로좀 (rat liver microsomes)에서 LB 의 안정성을 평가한 결과, LB 는 실험 시작 30 분 후, 약 56% 가 잔존하여 간에 의한 대사에 안정한 것으로 나타났다. 랫드 간 마이크로좀에 의해 생성되는 LB 의 대사체는 주로 demethylation 된 형태와 hydroxylation 된 형태로 확인 (metabolite identification)되었고, 이는 랫드 및 사람에서 형성될 수 있는 대사체를 파악하는데 중요한 정보를 제공하였다. 또한, 사람 CYP isozyme (CYP 1A2, 2C9, 2C19, 2D6 및 3A4)에서 각각의 기질 (substrate)과 LB 의 반응을 조사한 결과, CYP1A2, CYP2C9 및 CYP2C19 와 상호작용 (drug-drug interaction)하여 기질의 대사체 생성을 억제하였다.

LB 의 약물동태학적 특성을 파악하고자, 랫드에 0.5, 1 및 2 mg/kg 용량으로 정맥투여 또는 0.5 및 2 mg/kg 용량으로 경구투여하였다. 혈액 중 LB 의 농도는 fast-flow protein precipitation

(FF-PPT) 법으로 제단백을 실시한 후, LC-MS/MS 로 분석하였으며, 이 방법은 직선성, 정확성, 정밀성, 희석성, 회수율, 생체시료 영향(matrix effect) 및 안정성 항목에서 분석에 적합하였다. 정맥투여시 LB 의 약물동태는 선형 약물동태 (linear PK)양상을 나타내었으며, 경구투여시 약 95%의 높은 생체이용률 (bioavailability)을 나타내어, 대부분 체내로 흡수 (absorption)되는 것을 알 수 있었으며, 주로 간, 심장, 폐 및 지방으로 분포 (distribution)하였다. 그리고, 담즙, 뇨 및 변을 통한 배설 (excretion)과 소장관 (GI tract)에 존재하는 LB 가 투여량의 약 10 % 이하인 것으로 미루어, 주로 간에서의 대사 (metabolism)에 의해 소실되는 것으로 추정되었다.

TZD 계열 약물 LB 의 성간 차이 (gender difference)를 확인하고자, 수컷 및 암컷 랫드에 0.1-10 mg/kg 의 용량으로 경구투여를 실시한 결과, 암수 랫드의 혈중농도 – 시간 곡선하면적 (AUC)은 투여용량의 증가에 따라 용량상관적으로 증가하였으며, 투여용량별 AUC 는 암컷 랫드가 수컷 랫드보다 3.9-5.4 배 높았다. 이러한 결과는 LB 의 주요 소실경로인 간에서의 대사와 관련이 있을 것으로 판단되어, 암수 랫드

간 마이크로좀 (liver microsomes)에서의 LB 의 intrinsic clearance (CL_{int})를 평가한 결과, 암컷 랫드의 CL_{int} 가 수컷 랫드의 약 29% 로 나타났다. 이러한 결과는 랫드를 이용한 경구투여 약물동태실험에서 얻은, 암컷 랫드의 clearance (CL)가 수컷 랫드의 약 20%인 결과와 매우 유사하여, 암수 랫드의 체내 약물 흡수차이는 간에서의 대사와 관련이 있는 것으로 확인되었다.

이상의 결과를 종합해보면, LB 의 흡수, 분포, 대사, 및 배설의 체내속도 연구는 새로운 당뇨병치료제 LB 의 약물동태학적 특성 파악과 약물의 개발에 유용한 정보를 제공할 것으로 사료된다.

주요어: Lobeglitazone, p-glycoprotein, ADME, Pharmacokinetics, Transporters, CYP enzyme, Microsomal stability, LC-MS/MS

학번: 2007-30464